Description of GPS uncertainties within the Long Term Study on Anomalous Time-Dependent Subsidence

Simon Williams, National Oceanographic Centre – Liverpool

Literature Review of the Major Signals in GPS Coordinate Time Series

The first comprehensive study of the precision and accuracy of GPS coordinates was [*Larson and Agnew*, 1991] (with an acknowledgement to [*J. L. Davis et al.*, 1989]). They concluded that the short-term precision was on the order of 17 mm for the vertical and for long-term precision, 11.7 mm with a baseline dependence of 13 parts in 10^8. However at that time the GPS constellation was incomplete and measurements were made over a span of around 7-8 hours (at the most optimal time of day) on 4 – 5 consecutive days. The data was processed as baseline measurements and not converted to individual site coordinates (hence the baseline dependence). The small amount of data precluded any attempt to look at time dependence in the data.

Using continuous measurements of near surface monuments from a laser strainmeter in Southern California [*F Wyatt*, 1982] and [*F. K. Wyatt*, 1989] demonstrated that the power spectra had a power law dependence on frequency of the form

$$P(f) = \frac{P_r}{(2\,\pi f)^2} \tag{1}$$

In addition, [*John Langbein et al.*, 1993] showed that other geodetic measurements such as two-colour geodimeters, creepmeters and water wells also demonstrated an f^{-2} dependence in their power spectra. This behaviour is typically known as Brownian motion or random walk. [*Agnew*, 1992] showed that the spectra of many geophysical phenomena can often be approximated by a power-law dependence on frequency and introduced a more general form of the power spectra (following the work of [*Mandelbrot and Ness*, 1968]), given by

$$P(f) = P_0 \left(\frac{f}{f_0}\right)^{\kappa} \tag{2}$$

where P_0 and f_0 are normalising constants, f is the frequency and κ is the spectral index. [*Johnson and Agnew*, 1995] demonstrated the effect long-range time dependent correlations have on the estimates of uncertainty, primarily that neglecting such behaviour leads to estimates of the uncertainty that are overly optimistic (too small). They argued that if this random walk motion seen in geodetic data is related to monument motion then it is an issue for all geodetic instruments.

Using Maximum Likelihood Estimation (MLE) [*J. Langbein and Johnson*, 1997] estimated the amplitudes of random walk and white noise in the time series from two-colour EDM (geodimeter) measurements. They found that the random walk noise level averaged about 1.3 mm/√yr with a range between 0 and 4 mm/√yr. The first paper to examine time-correlated noise in GPS data was [*N E King*

et al., 1995]. They found no evidence of random-walk noise in the time series but did find some evidence of short-term correlation of around 25 days from the autocorrelation function. The amount of white noise in the series was found to be on the order of 5 mm in the vertical. However only one baseline was analysed and it was 2 ½ years in length. They concluded that the random walk noise might simply be undetectable at that point.

In addition to temporally correlated noise, GPS time series were also identified as containing a spatially correlated, common mode [*Wdowinski et al.*, 1997]. This to some extent has divided GPS time series analysis into two categories, global and regional (or unfiltered and filtered respectively). Where there is a network of sites with sufficiently small baselines the common mode signal can be removed by a variety of methods such as stacking of the residuals [*Wdowinski et al.*, 1997], principal component analysis [*Serpelloni et al.*, 2013] or by the use of defining a regional reference frame and fitting and applying a daily Helmert transformation [*Hurst et al.*, 2000]. In general a globally distributed set of sites are sufficiently separated that they may be considered to be uncorrelated from each other and the common mode noise cannot be reduced and the noise is typically higher than the filtered (regional) series.

[*Zhang et al.*, 1997] examined 19 months of continuous GPS (CGPS) data from 10 sites in southern California. Since a common mode signal was removed the results were for a regional, filtered network. They used MLE, autocorrelation analysis and power spectra to analyse the time series. For the MLE analysis they chose three candidate models; white noise only, white noise plus flicker noise [*Voss and Clarke*, 1975] (κ = -1) and white plus random walk noise. They found that the flicker plus white noise model best described the data. The average amplitudes for the vertical component was 6.8 ± 0.6 mm (95% confidence) for the white noise and 6.2 ± 2.7 mm [sic] (95% confidence) for the flicker noise (Note that in this paper they used an approximation for the flicker noise covariance and so the amplitudes may not be comparable to later papers). By fitting a straight line to the power spectra (in log-log space) they obtained a median spectral index of -0.4. [*Mao et al.*, 1999] examined a globally distributed set of 23 sites that contained 3 years of data. They also used a combination of power spectra and MLE with integer spectral indices and concluded that white plus flicker noise best described the noise content of the series. In the vertical the mean white noise and flicker noise amplitudes were 10.3 mm and 14.7 mm respectively. The mean spectral indices, estimated from the power spectra, ranged from -0.74 to -1.02. They also found that the white noise component had a latitude dependent bias in the vertical (noisier at the equator). [*Calais*, 1999] confirmed the above results (in the horizontal only) using three permanent sites in Europe as did [*Caporali*, 2003] who used the two-sample Allan variance [*Allan*, 1966] to study the noise characteristics of 21 sites from the EUREF network with time spans ranging from 3 to 6 years. [*Caporali*, 2003] also found very little evidence of random walk noise in the time series.

While most of the earlier studies concentrated on the integer spectral indices as potential stochastic models, primarily because their knowledge on how to create covariance matrices was limited to flicker and random walk noise, there is no reason why a non-integer spectral index may not be more appropriate. Indeed the spectral indices estimated from fitting a line to the power spectra highlighted a range of non-integer values but invariably close to, or slightly lower (closer to zero), than -1. [*S.D.P. Williams*, 2003] introduced the fractional differencing method of [*Hosking*, 1981] which allowed one to produce a covariance matrix for a power-law noise with any spectral index and therefore the ability to estimate the spectral index in addition to the noise amplitudes using MLE. [*S.D.P. Williams et al.*, 2004] analysed a total of 954 continuous GPS position time series, with lengths from 16 months to 10 years, from 414 individual sites in nine different GPS solutions (both regional and global solutions) to produce the most comprehensive study of noise content so far. They used two MLE approaches to

study the data; the traditional method of assuming white noise, white plus flicker noise and white plus random walk and a second analysis where the spectral index and amplitude of the power-law noise were estimated simultaneously with the white noise. For the global solutions the mean spectral index for the vertical component was found to be -0.8 ± 0.4 which was therefore consistent with a flicker plus white noise model (which was the most likely model in the integer analysis also). Both noise components showed a latitude dependence on their amplitudes (higher at equatorial sites) together with a bias to larger values in the Southern Hemisphere. The flicker noise amplitude was 20.2 mm/yr^{¼} and 23.1 mm/yr^{¼} (SOPAC and JPL solutions respectively) and the white noise amplitudes were 3.9 mm and 7.7 mm. The noise was found to be significantly lower in the in the regional filtered solutions and the estimated spectral index was found to be more varied than the global solutions but they were still centred around a value close to flicker noise. The average noise amplitudes in the vertical were 7.9 mm/yr^{¼} for the flicker noise and 3.2 mm for the white noise. A significant reduction in the noise amplitudes could also be seen since the first CGPS networks began in the early 1990's. They also divided the GPS sites into different monument types and found that the deep drilled braced monument design offered the lowest noise levels.

The papers since [*S.D.P. Williams et al.*, 2004] all tend to confirm the same results that a suitable noise model for CGPS coordinate time series is a flicker plus white noise model. The average parameters from the major studies are shown in the table below. We note that a) the more recent studies tend to have longer time spans and more sites; b) the noise amplitudes have reduced and c) the presence of random walk is still unconfirmed.

Table 1. Means and Standard Deviations of the White Noise and Flicker Noise Estimates for the vertical Component from various studies. Also Included is the Approximate Time Span of Data Used, the Number of Sites and any Estimate of Spectral Index.

Study	Global or Regional	White noise amplitude (mm)	Flicker noise amplitude (mm/yr^{¼})	Time span of data	Number of sites	Estimated spectral index
[*Zhang et al.*, 1997]	Regional	6.8 ± 0.6	6.2 ± 2.7	1.6	10	-0.4
[*Mao et al.*, 1999]	Global	10.3	14.7	3	23	-0.72, -1.02
[*S.D.P. Williams et al.*, 2004]	SOPAC Global	3.9 ± 1.9	20.2 ± 5.5	3.6	207	-0.8 ± 0.2
	JPL Global	7.7 ± 2.6	23.1 ± 7.8	2.5	268	-0.8 ± 0.3
	SOPAC SCIGN (R)	3.0 ± 0.5	7.0 ± 5.0	2.7	147	-0.9 ± 0.5
	JPL SCIGN (R)	3.6 ± 0.9	7.0 ± 3.2	2.2	58	-1.0 ± 0.7
	USGS SCIGN (R)	4.1 ± 1.0	9.2 ± 3.7	2.5	112	-0.8 ± 0.4
	PANGA PANGA (R)	5.0 ± 1.9	12.5 ± 4.9	3.9	54	-0.7 ± 0.3
	SOPAC PANGA (R)	2.4 ± 0.7	8.6 ± 4.0	4.4	30	-0.9 ± 0.3
	SOPAC BARGEN (R)	2.3 ± 0.6	5.5 ± 2.2	4.7	47	-0.9 ±0.4
	REGAL REGAL (R)	4.2 ± 1.1	10.9 ± 5.5	4.0	31	-0.9 ± 0.4
[*Beavan*, 2005]	Global	3.7 ± 0.8	8.5 ± 2.6	4.1	15	
[*A R Amiri-Simkooei et al.*, 2007]	Global	5.4 ± 0.6	9.3 ± 0.7	10	5	
[*J. Langbein*, 2008]	SCIGN (R)	2.3 ± 0.5	4.6 ± 1.3	3.5-10	210	
	BARGEN (R)	2.3 ± 0.3	3.6 ± 1.1	3.5 – 10	26	
[*Teferle et al.*, 2008]	Global	3.1 – 5.3	10.9 – 20.4*	4	6	-0.4, -1.2
[*Santamaría-Gómez et al.*, 2011]	Global	1.9 ± 0.1	5.8 ± 0.1	2.5 – 13	275	-0.88 ± 0.02
[*Serpelloni et al.*, 2013]	Global	2.4 ± 1.1	12.2 ± 3.1†	2.5-14	>800	-0.7
	Regional	5.6 ± 0.7	7.4 ± 3.1†	2.5-14	>800	

* These are for power-law noise and not flicker noise but should be close; † These were calculated with another software which scales the amplitudes different – they have been converted to be the same as CATS. See Appendix A.

[*Calais et al.*, 2006] looked at sites in the North American Plate interior and estimated the random walk noise amplitudes using MLE and assessed them against their monument class (sites whose monuments are suitable for tectonic studies such as braced monuments, pillars, bedrock, anchored pillars etc. and those that are not suitable such as rooftops and fence posts). They found random walk amplitudes on the order of a few mm/yr^{½} to 10 mm/yr^{½} and found that the tectonically suitable monuments performed slightly better. However they did not estimate the amount of flicker noise in the time series so the random walk amplitudes will be biased high by neglecting this noise. [*A R Amiri-Simkooei et al.*, 2007] used a different technique to MLE, least-squares variance covariance estimation (LS-VCE) but came up with similar results to MLE. As well as increasing the number and time span of series examined, different stochastic models have been introduced as candidates. [*J. Langbein*, 2004; 2008] introduced First-Order Gauss Markov noise (equivalent to an autoregressive noise of order 1), a Generalised Gauss Markov noise, Bandpass noise (due to spectral leakage around a certain frequency such as the annual) and multiple combinations of these and the more usual power-law models. No model has stood out as being more suitable for GPS coordinate time series. Generally we find that series are distributed amongst the various model combinations most likely indicating that the data is not sufficiently long enough to allow such increases in the degrees of freedom of the model to choose a preferred model. [*Santamaría-Gómez et al.*, 2011] following on from [*Simon Williams and Willis*, 2006], who were examining DORIS data, tested two alternative white noise models, time variable white noise (where the white noise amplitude is allowed to reduce with time) and variable white noise (where the daily formal errors are used and you solve for a variance scale parameter). In all they tested 27 different stochastic models (mainly different combinations of 7 models). They found that any combination of coloured noise with variable white noise was significantly superior to the simple white noise model and the time-variable white noise.

[*J. Langbein*, 2008] examined the time series from 236 sites in Southern California and Southern Nevada. He found that the sites with the smallest errors were those in Nevada (dry desert) with deeply braced monuments. Sites that were installed within regions of active pumping of both oil and groundwater had the largest errors. More recent papers tend to focus on regional networks (either filtered or unfiltered) and have confirmed the previous findings (for example, [*Serpelloni et al.*, 2013], [*Khan et al.*, 2010]). Most of these papers have used MLE (and the related LS-VCE) as the estimation method. However, others have tried more heuristic methods to analyse the time series. [*Hackl et al.*, 2011], [*Caporali*, 2003] and [*Niu et al.*, 2014] have used the Allan variance whereas [*Bottiglieri et al.*, 2010] used Independent Component Analysis and [*Khan et al.*, 2010] in addition to using MLE also looked at the series autocorrelation. [*Olivares and Teferle*, 2013] used Bayesian Monte Carlo Markov chains to study the time series whereas [*Montillet et al.*, 2013] used Negentropy and Empirical Mode Decomposition. However, none of the results differ from what was found using the traditional MLE method.

Recently, [*Dmitrieva et al.*, 2015] used a combination of MLE and a Kalman filter to estimate a network-wide estimate of noise in GPS time series. Only one estimate of the amplitudes of the noise was estimated. Using 15 sites from central eastern USA they found random walk of 0.82 mm/yr^{½} alongside flicker white noise (with amplitudes 4.0 mm/yr^{¼} and 1.1 mm respectively) in the horizontal but no random walk in the vertical component (the flicker noise and white noise amplitudes were 7.9 mm/yr^{¼} and 2.3 mm respectively). The random walk amplitude is at the low end of that found from other geodetic data but at the high end of results found from short baseline studies (see below).

Short Baseline Studies

In order to better isolate site-specific effects several authors have analysed long running, short GPS baselines (< 1km) to take advantage that certain errors such as satellite orbit, residual troposphere and ionosphere are differenced to negligible levels. Using a dense network of sites with braced monuments at Yucca Mountain, Nevada [*Hill et al.*, 2009] found root mean square residuals of 0.20-0.72 mm for the vertical component (no attempt was made to look at temporal correlations) and found a correlation in the seasonal cycle that lagged local temperature measurements by about a month. They suggested this could be related to bedrock thermal expansion. [*M A King and Williams*, 2009], using 10 short baselines, found white noise on the order of 0.18 mm in the vertical and flicker noise with an amplitude of 1.85 mm/yr^{¼}. They also placed a loose constraint on the order of any random walk noise due to monument instability at around 0.5 mm/yr^{½} for a baseline. They also found annual variations that correlated well with temperature data but a simple model of linear thermal expansion could only explain the signal at one baseline. Further they also found spurious trends over 0.5 mm/yr that may be explainable as a combination of near field multipath and changing satellite geometry.

Periodic Signals

GPS site coordinates are naturally subject to periodic signals from a variety of sources. [*Mao et al.*, 1999] noted that peaks in the power spectra were clearly visible at annual and semi-annual periods for some sites. A large component of signals at annual and semi-annual periods are known to be true physical motion [*Blewitt and Lavallee*, 2002; *Van Dam et al.*, 2001] and are due to surface loading due to hydrology, atmospheric and ocean bottom pressure. [*Blewitt and Lavallee*, 2002] found typical amplitudes of 4 mm for the vertical in the annual and 1.5 mm for the semi-annual. However [*Dong et al.*, 2002] found that less than half of the power observed at the annual period can be explained by seasonal surface mass redistributions and concluded that the remainder must be due to unmodeled wet tropospheric effects, bedrock thermal expansion, satellite orbits and phase centre variation models. Spurious long period signals can also occur due to aliasing of tidal signatures [*Penna and Stewart*, 2003; *Penna et al.*, 2007]. A prominent 13.6 day peak in the power spectrum of the common mode noise was seen by [*S.D.P. Williams et al.*, 2004] and attributed to tidal aliasing. Using 167 sites from the International GNSS Service (IGS) network, [*Ray et al.*, 2008] found anomalous harmonics in the spectra at 1.040 ± 0.008 cycles per year (up to around the 6th harmonic) which is close to the repeat period of the GPS constellation of 351.2 days. These harmonics of the GPS "Draconitic" year have also been found by [*A R Amiri-Simkooei et al.*, 2007; *Santamaría-Gómez et al.*, 2011] amongst others. The effect an annual signal (or any long period signal) has on estimated trends if they are unaccounted for was studied by [*Blewitt and Lavallee*, 2002; *M S Bos et al.*, 2010] and they recommended that 2.5 years be adopted as a standard minimum span for estimating trends. Below 2.5 years the velocity can be biased to an unacceptable level. This however is only true in the case when no annual signal is estimated. [*James L. Davis et al.*, 2012] explored the implications that seasonal signals may not be pure sinusoids with a constant amplitude and phase and suggested that some of the noise in GPS time series might be due to neglecting the variability of the seasonal signal. However their seasonally derived stochastic model (similar to the annual band-pass noise explored by [*J. Langbein*, 2004; 2008]) would always lead to a flat spectrum at frequencies lower than the annual; something that has not been seen in GPS time series so far (see Figure 2 of [*Ray et al.*, 2008] for example). It is likely

that it forms some part of the noise characteristics of GPS time series but not at a sufficiently large level to be the main cause of the time-correlated noise.

Offsets

It is well known that GPS coordinates time series are disrupted by offsets (sharp change of the mean) that can be broadly categorized into actual crustal movements, mainly earthquakes, or artificial events such as environmental, equipment malfunction and change or human error that either occur at known (such as documented equipment changes) or unknown times with sizes that are, at best, known very imprecisely. A thorough investigation of offsets in GPS time series was performed by [*S. D. P. Williams*, 2003]. He showed that on average one offset occurs on a component by component basis every 9 years (but this could be as frequent as one in every 2 years) and that undetected offsets in the time series can mimic random walk behaviour. Following on from this [*Gazeaux et al.*, 2013] reported on the results of the Detection of Offsets in GPS Experiment (DOGEx) which was used to test the effectiveness of various methods used by different groups to detect and remove offsets. They found that currently, manual methods were superior to any automatic solution. They also noted from analysing the SOPAC archive (the Scripps Orbit and Permanent Array Center) that out of all noted offsets 33% were unknown, 34% due to a seismic event and 29% attributed to equipment change. Finally [*F.K. Wyatt and Agnew*, 2005] studied the baseline between two continuous GPS sites at Pinon Flat Observatory in southern California, PIN1 and PIN2, which are some of the oldest continuous sites having begun measuring in the early 1990's. The records for these sites have been meticulously maintained and many experiments were performed there to test the equipment. As mentioned above the baseline analysis of these two sites reduces the noise by up to an order of magnitude allowing offsets of the order of 1 mm or less to be detected and attributed to such changes as simple removing and replacing the same antenna. Such offsets would not be visible in a normal individual coordinate time series.

Campaign Measurements

Very little work has been done on the noise uncertainties of campaign GPS and there is no real defining paper on the subject. In general the noise at a campaign site should be no different than at a continuous GPS site apart from two obvious differences. First, campaign measurements may use ordinary tripods during the measurement campaign (which may or may not consist of a full 24 hour dataset) and therefore no permanent anchorage to the solid bedrock. It would therefore be difficult to assess monument motion in the same manner as for the permanent sites. Secondly, the antenna and tripod (where used) will be installed over a benchmark during every campaign. Theoretically this should lead to an additional "set-up" noise that would only manifest itself in continuous data at the start of the measurements and when there was a change in the antenna/monumentation at the site. We have no knowledge of the size of this set up noise and it would likely be operator dependent. We know from [*F.K. Wyatt and Agnew*, 2005] that removing and replacing the antenna can produce offsets on the order of a few mm. Factoring in uncertainties in measuring the height of the antenna above the benchmark which is also likely to be on the order of a few mm. [*Arianna Pesci et al.*, 2009; *A. Pesci et al.*, 2010; *Teza et al.*, 2010] have produced the most comprehensive work on this so far. They use simulated data with noise equivalent to continuous GPS (or real data from sites close to the

campaign site) and add an additional noise to account for the "set-up" noise (which is white noise per individual campaign) and run Monte Carlo simulations to estimate the trend uncertainties. The only unknown is the size of this "set up" noise. An experiment where campaign sites were set up and removed over a number of weeks with a very close permanent site(s) in order to produce baseline solutions is the likely way to go forward.

Conclusions

There is an extensive body of literature examining the stochastic noise in GPS coordinate time series and other major effects expected to have an effect when attempting to measure trends, changes in trends and their associated uncertainties. The predominant finding is that GPS coordinates are correlated both spatially and temporally and that an appropriate model is a combination of flicker noise and white noise (or potentially white noise and power-law noise with a spectral index close to -1 or slightly lower). The origin of this noise is still unknown but we do know that over time both the amplitude of the white noise and the time-correlated noise has reduced in size pointing at least partly to something that is not purely physical (e.g. tropospheric or ionospheric) but related to the improvements in the processing algorithms, the satellite geometry and the number of GNSS sites available. Random walk, which is attributed to motion of the monument, has not been categorically proven so far. If it does indeed exist that it should be lower than 1 mm/yr^{½} at well-designed sites. A conservative value to use may by the 0.82 mm/yr^{½} found by [*Dmitrieva et al.*, 2015]. Another good review on some of the issues for GPS coordinates is given by [*M King et al.*, 2010]. The size of the noise is dependent on the type of network you have from global, through to filtered regional and short baseline solutions, the noise decreases respectively. The noise amplitudes have also steadily reduced in time. When estimating the trends of the continuous and campaign GPS the noise amplitudes and models should be derived from the long continuous sites to provide the best, most realistic stochastic model for the project. In terms of the campaign measurements we should use the models derived from the continuous results and factor in an additional set up noise with a best guess estimate of the amplitude.

Stochastic Modelling of GPS time series

Methods

There are many different methods in the scientific literature for estimating and qualifying temporal correlations in time series. Many of these methods are heuristic in nature such as Allan variance, detrended fluctuation analysis, power spectral analysis, variograms. Others such as Maximum Likelihood Estimation (MLE) and Variance-Covariance Estimation are more parametric [*Beran*, 1994]. Often the objective of the statistical analysis is not to show that there are time correlations in the data but to characterize it in order to understand its behaviour regarding other parameters and their uncertainties estimated from the time series. In this work we use one heuristic method, Power Spectral analysis and one parametric method, MLE, to produce a realistic stochastic model for the permanent monitoring stations based on the analysis of the vertical time series provided, inference from comparison with time series from stations in Netherlands processed by other groups using established scientific processing software and comparison with past analysis of GPS time series (see literature

review above). Power spectra are well known methods for examining time series in the frequency domain. They measure the amount of a signal's power occurs in a given frequency band. We use here the redefined periodogram [*Scargle,* 1982] (and its equivalent for continuous data using FFT's) to evaluate the power spectrum of the time series. Power spectra are useful visualization tools because many stochastic models have a simple functional relationship to frequency (for example, equations 1 and 2 above), significant periodic signals are easy to identify and the overall scale of the process can be evaluated.

We will use Maximum Likelihood Estimation as described by [*J. Langbein and Johnson,* 1997; *Mao et al.*, 1999; *S.D.P. Williams et al.*, 2004; *Zhang et al.*, 1997] to evaluate the amplitudes and type of stochastic model present in the GPS time series. Importantly, for reasons explained further below, we employ the methods, algorithms and stochastic models introduced in [*M Bos et al.*, 2008; *M S Bos et al.*, 2013; *M S Bos et al.*, 2014]. First, we will give a very brief introduction to MLE to facilitate the interpretation of the results.

Given a Gaussian data vector, **x**, the joint distribution function for a given covariance matrix, C, is equal to

$$lik(\,x, C) = \frac{1}{(2\pi)^{\frac{n}{2}}(\det C)^{1/2}} \exp\left(-\frac{1}{2}x^t C^{-1}x\right) \tag{3}$$

where *n* is the number of data and det is the matrix determinant. The log-likelihood function is given by

$$\ln[lik\ (x, C)] = -\frac{1}{2}[\ln(\det C) + x^t C^{-1}x + n\ln(2\pi)] \tag{4}$$

where ln is the natural logarithm. The covariance matrix is adjusted until the likelihood estimate is maximised. In addition, since the data vector **x** is the residual from a linear model typically including an intercept, secular rate (or rates), offsets and periodic signals, these parameters need to be evaluated alongside the estimated covariance matrix. The data residuals, **x**, are related to the design matrix, *A*, the original data **x'** and the estimated model parameters, *m* by

$$x = x' - Am \tag{5}$$

using the weighted least squares formula

$$m = (A^T C^{-1} A)^{-1} A^T C^{-1} x' \tag{6}$$

The data covariance matrix, in GPS time series analysis [*J. Langbein and Johnson,* 1997; *Mao et al.*, 1999; *Zhang et al.*, 1997] typically takes the form

$$C = \sigma_{wh}^2 I + \sigma_{rw}^2 C_{rw} + \sigma_{fl}^2 C_{fl} \tag{7}$$

or

$$C = \sigma_{wh}^2 I + \sigma_{pl}^2 C_{pl} \tag{8}$$

where I is the n x n identity matrix representing the unit covariance matrix for white noise (no cross correlation), C_{rw}, C_{fl} and C_{pl} are the unit covariance matrices for random-walk, flicker or any other temporally correlated noise (often power law noise with a spectral index, κ) respectively and σ^2 representing the variance of the various stochastic models.

The likelihood function is typically maximised using a function such as the uphill simplex or Brent algorithms. If we wish to test between competing models of the covariance matrix or different linear models, *A*, then we can compare the ML values. However this does not take into account the complexities of the different models (number of estimated parameters both in the linear and the stochastic model). A better test is to use the Bayesian Information Criteria (BIC) which is defined as

$$BIC = -2\,MLE + k\ln(n) \tag{9}$$

where *MLE* is the maximum likelihood estimate, *k* is the number of estimated parameters (both linear and stochastic). If the number of parameters between different models remains equal then the BIC is equal to the MLE.

There are three main, computationally intensive, parts to this problem: the computation of the determinant of the covariance matrix, the weighted least squares and the inverse of the covariance matrix. If the MLE is performed in a high-level, numerical computation language such as matlab then the three parts can be computed as shown in the equations. However there are different methods for obtaining the individuals parts which are computationally faster (up to O (n log n) instead of O (n^3)) and often have greater numerical stability. These often depend on the form of the covariance matrix and are discussed to some extent in [*M Bos et al.*, 2008; *M S Bos et al.*, 2013; *M S Bos et al.*, 2014].

Stochastic Models

As can be seen from above, MLE relies on the choice of stochastic models available (of which there is a huge variety) that can be formulated to create a covariance matrix. BIC can then be used to test between competing models and between combinations of models. Perhaps the most common stochastic model in geophysics is the power-law model as described by equation 2. It is related to fractals and fractional Brownian motion. Power law models where the spectral index is an integer have been given names such as random walk (κ = -2), flicker noise (κ = -1), and white noise (γ = 0). Another common model, particular in statistics, is the autoregressive model : primarily the autoregressive one parameter model (AR(1) or sometimes known as First-Order Gauss Markov noise) due to its ease of implementation. In terms of power spectrum an AR(1) model has a slope of -2 at high frequencies and a slope of 0 at low frequencies. The cross-over frequency depends on the single parameter, γ. [*M S Bos et al.*, 2014] (re) introduced some other useful models. The first, an autoregressive fractionally integrated (ARFI) model has a change in the power law slope related to γ where the difference between the slopes on either side of the cross-over frequency is always 2 but the whole spectra is tilted by κ. So if the low frequency spectral index is -1, then the high frequency spectral index would by -3. A Generalised Gauss Markov, first introduced by [*J. Langbein*, 2004], is similar to an AR(1) except the spectral index above the cross-over frequency can take any spectral index, κ. However, the spectral index below the cross-over frequency is always 0. We introduce here a new model, the Fractionally Integrated Generalised Gauss Markov (FIGGM), which combines the GGM model and fractional integration (which forms power-law noise: comes from the fact that

integrating white noise produces random walk noise) which can be defined by three parameters, κ_L, κ_R and γ; a spectral index below (to the left) the cross-over frequency, a spectral index above (to the right) of the cross-over frequency and a parameter, γ ($0 \rightarrow 1$), that defines where the cross-over frequency lies. As γ tend to 1 the cross-over frequency decreases in frequency. The FIGGM model is useful in that all of the above models are subsets of this model.

Permanent GPS Data

The primary dataset supplied by NAM are the time series from 20 permanent stations in northern Netherlands (Figure 1 below). The processing was carried out by 06-GPS using the GNSMART software by Geo++ GmbH. The description of the methodology is given in the project report (Geo++ Anjum continue GPS test NAM447_4.pdf with addendum: Continuous Object Monitoring withh Gps.pdf).

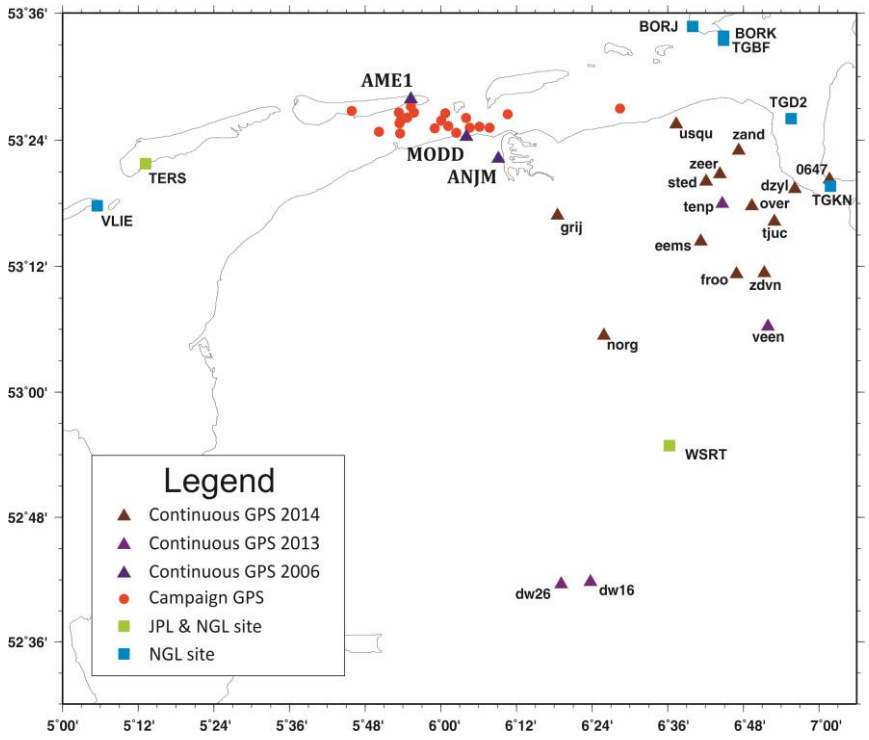

Figure 1. Map of the GPS sites used in this study. Triangles indicate the permanent sites provided by NAM and processed by 06-GPS. Squares indicate permanent sites that have been processed by the Jet Propulsion Laboratory and Nevada Geodetic Laboratory. Circles indicate the position of some of the campaign sites.

The main feature of this processing to note is that the approach uses a Kalman filter with a 12 station (not consistent throughout the time period) network of reference sites that are held "fixed". These fixed stations are processed annually (with six weeks of data) in a separate processing stream where thier positions are relaxed to allow changes in their coordinates. If the coordinates change beyond a pre-defined threshold then the reference coordinates are updated and used in future processing updates. The coordinates are sampled to hourly intervals which is unusual with respect to the scientific community which typically uses intervals of days and sometimes weeks. Of the 20 permanent stations only three (AME1, MODD and ANJM) date back to 2006 and have a long time series that is preferable for a thorough time series analysis.

Reference time series for comparison

In order to aid the interpretation of a suitable stochastic model we have supplemented the above dataset with other useful reference time series. In addition to the 20 permanent sites, 06-GPS has also provided a reference time series for the ITRF station Westerbork which is 450 days long. The Nevada Geodetic Laboratory (NGL) at the University of Nevada, Reno, the geodetic group at the Jet Propulsion Laboratory (JPL) and the Scripps Orbit and Permanent Array Centre (SOPAC) all produce time series for continuous sites around the global. Useful sites in the region from JPL and NGL are also plotted in Figure 1. JPL and NGL both use the GIPSY/OASIS software whereas SOPAC uses the GAMIT/GLOBK software. Figure 2 shows four time series for the Westerbork site. It is plainly clear that the 06-GPS site coordinates are more precise than the daily GPS solutions from the research groups (however that does not imply they are more accurate) and is clearly a result of the constraints imposed by the Kalman filter and the fixing of the reference stations. The same conclusions was seen when the 06-GPS solutions for AME1, ANJM and MODD were compared to the Leica CrossCheck results which uses the Bernese software (see the document "Crosschecking the GPS Leica CrossCheck service" for more details). Another thing to note is the similarity between the JPL and NGL solutions that both use GIPSY whereas the SOPAC solution which uses GAMIT/GLOBK is less similar and appears to have a larger annual signal compared to the others.

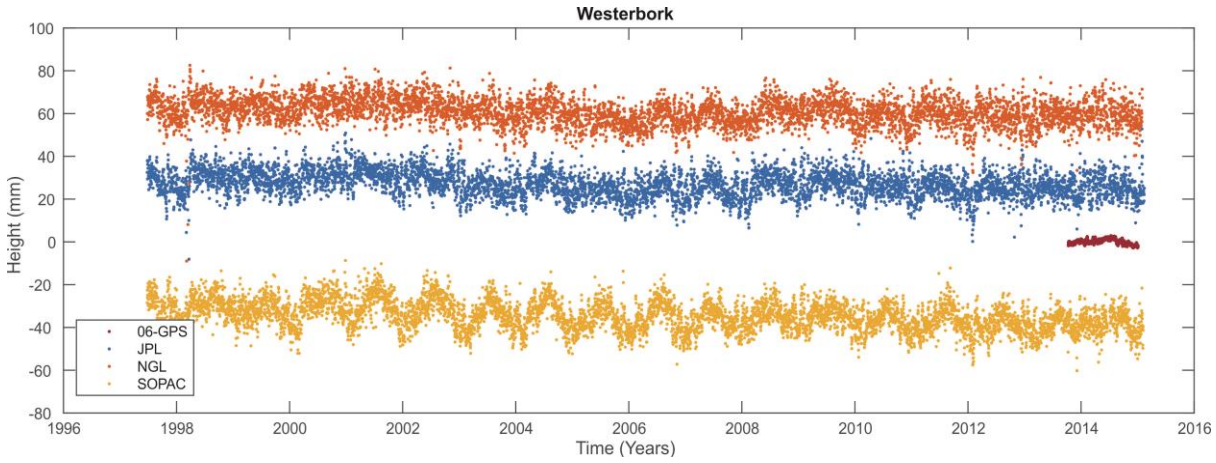

Figure 2. The vertical coordinate time series for the ITRF site Westerbork from different GPS solutions.

For the remainder of the stochastic modelling we will concentrate on the three longest sites: AME1, ANJM and MODD in the Waddenzee but supplement and compare those with results from the NGL solutions.

Power Spectral Analysis

The power spectra from the three longest sites are plotted in Figure 3. Also shown is the stacked (averaged) power spectrum from all 20 continuous sites. Note that this plot is in log-log form so that any power-law process will show as a straight line in the figure. White noise for instance would show as a flat spectrum (slope of 0) whereas random-walk noise would show increasing power at low frequencies with a slope of -2. We see that the spectra from AME1, ANJM and MODD and the averaged power spectrum all show power-law dependence and peaks relating to various tidal

frequencies. Also shown is the power-spectrum for power-law noise with an index of -1.88. This is a good fit to the observations at high frequencies but appears to overestimate the power at periods lower than around 10-20 days (~ $6e^{-7}$ Hz). At lower frequencies the spectra appear to have a different, lower, power-law dependence that looks to be a good candidate for a FIGGM model. Also evident is the lack of a white noise floor at the highest frequencies (there is a little flattening of the spectra close to the Nyquist frequency but that is related to the discretization of the data).

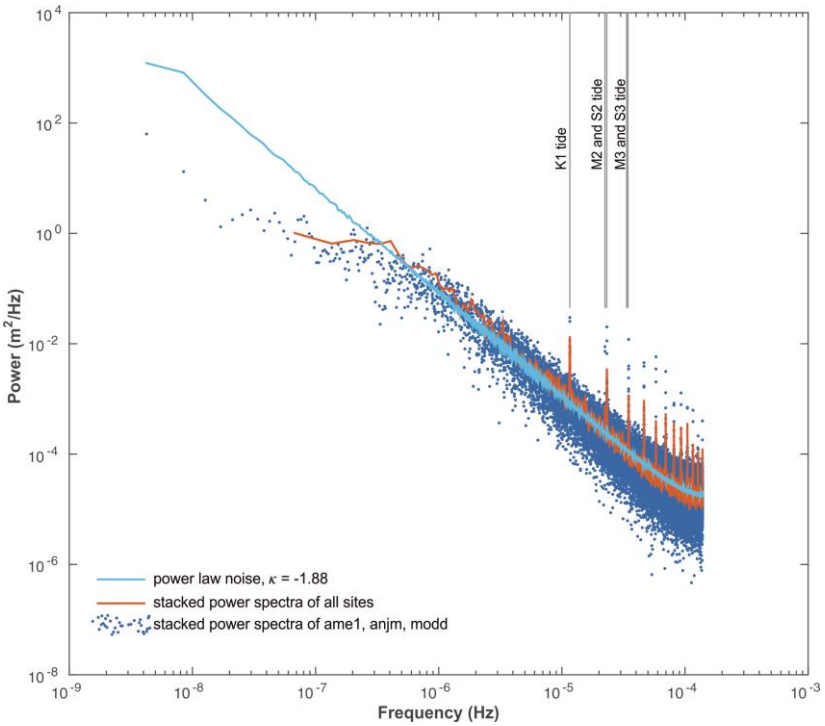

Figure 3. Power Spectra of the hourly time series. Blue dots represent the combined spectra from the longest sites: AME1, ANJM and MODD. Orange curve is the averaged spectrum from all 20 sites. Light blue curve is a synthetic power spectrum for power-law noise with a spectral index of -1.88. Light grey lines are some representative positions of tidal peaks.

The power spectra for the three longest sites are also shown with more detail in Figure 4. Included on the figures are some representative spectra so that the 06-GPS time series can be placed in context with previous studies. The red line on each plot is the spectra derived from the ML fit to the hourly data (see MLE section below) and the yellow line is the spectra from a power-law ML fit to the data. The blue line is the average from the ML fit to 11 NGL sites in the region (unfiltered) and the green line is the ML fit to the same sites after an average common mode signal has been removed (filtered data) and a representative curve for the filtered noise model from Table 1. The purple line characterizes the spectra from short baseline studies [*Hill et al.*, 2009; *M A King and Williams*, 2009] and the grey lines are spectra for random-walk noise at levels suspected to be due to monument motion; 0.5 mm/√yr [*M A King and Williams*, 2009] and 2 mm/√yr [*J. Langbein and Johnson*, 1997].

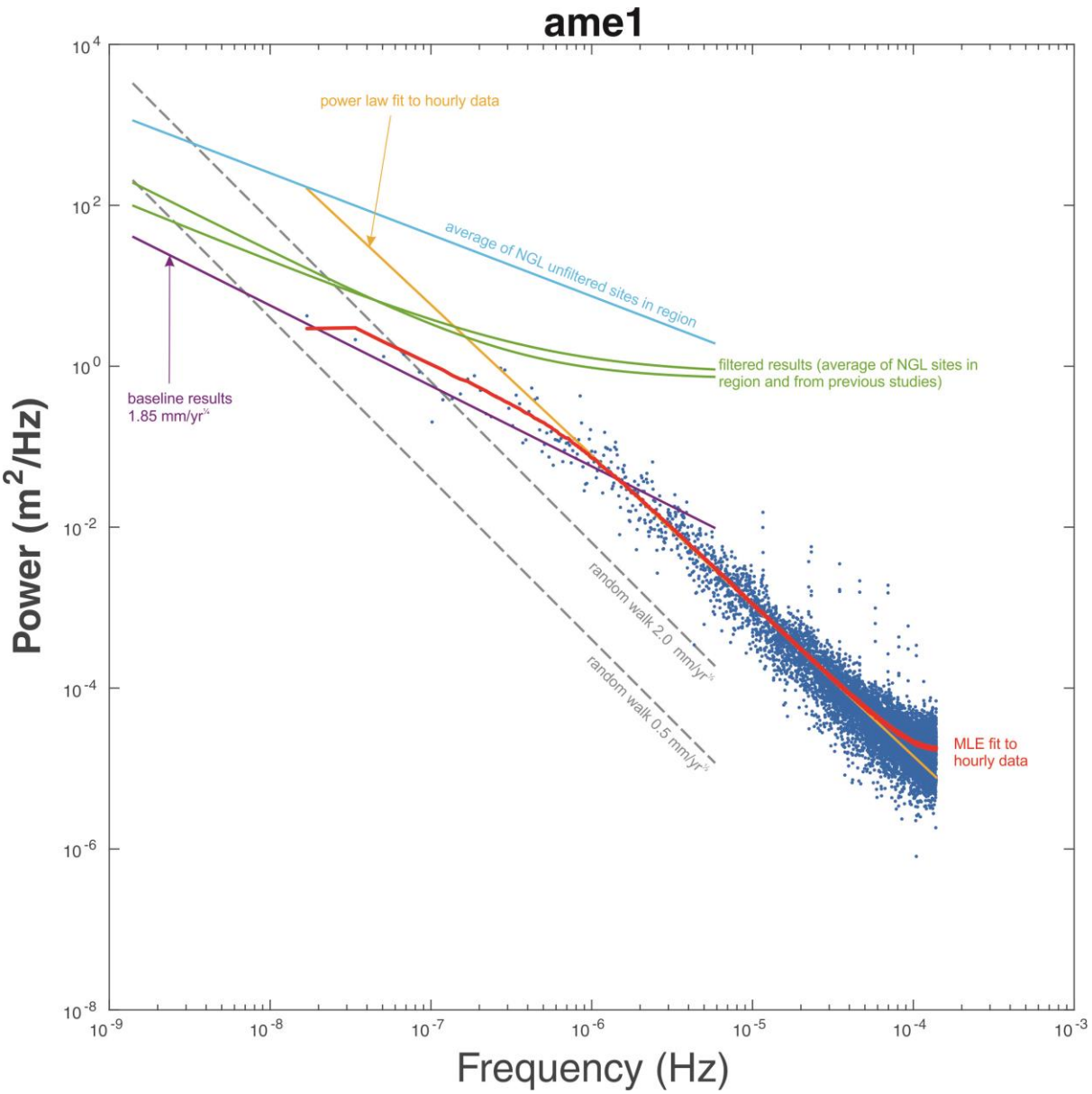

Figure 4a. Power Spectrum for site AME1 (blue dots). Also included on the plot is the spectrum derived from the MLE analysis (below) and some representative spectra from the literature review and the NGL time series in the region.

We note the following observations:

- The power of the hourly data is significantly lower at all frequencies than the unfiltered results from the geodetic research groups (as also witnessed visually in Figure 2).
- The power is lower than the filtered (regional networks) and does not show a similar white noise limit at high frequencies.
- The power at low frequencies (below 10-20 days) is similar in amplitude to the short baseline studies.
- The power-law slope at low frequencies is similar to the baseline, filtered and unfiltered results.
- At high frequencies the power-law slope is close to -2 which could be interpreted as monument motion. However if it was it would be much greater than previously encountered and would likely be visible in baseline and filtered studies.
- The slope and power of MODD at low frequencies are larger than ANJM and AME1.

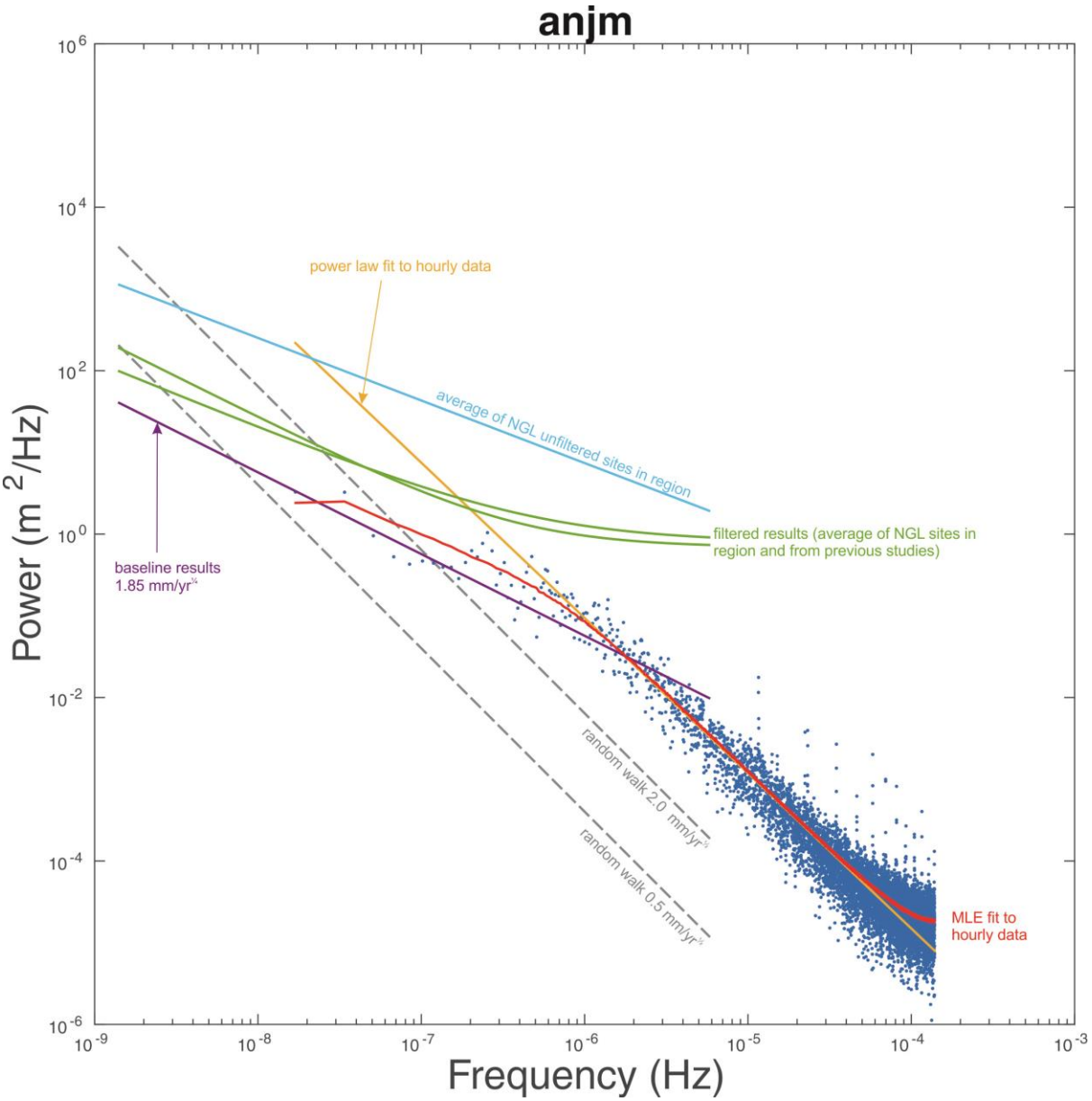

Figure 4b. Power Spectrum for site ANJM (blue dots). Also included on the plot is the spectrum derived from the MLE analysis (below) and some representative spectra from the literature review and the NGL time series in the region.

The close to random-walk behaviour at high frequencies is therefore unlikely to be due to monument motion but is likely due to the Kalman filtering which will constrain the coordinates stochastically as a random walk. How much this constraint affects the series at low-frequencies, where subsidence and time-varying subsidence effects are to be seen, is unknown. Given the good agreement found between the Leica CrossCheck and the 06-GPS results for AME1, ANJM and MODD (particularly the differenced results to MODD – similar to but not exactly equivalent to the baseline and filtered results) we will proceed to produce a realistic stochastic model from these three sites that can then be applied to the rest of the continuous sites and use it to produce a model for the campaign sites.

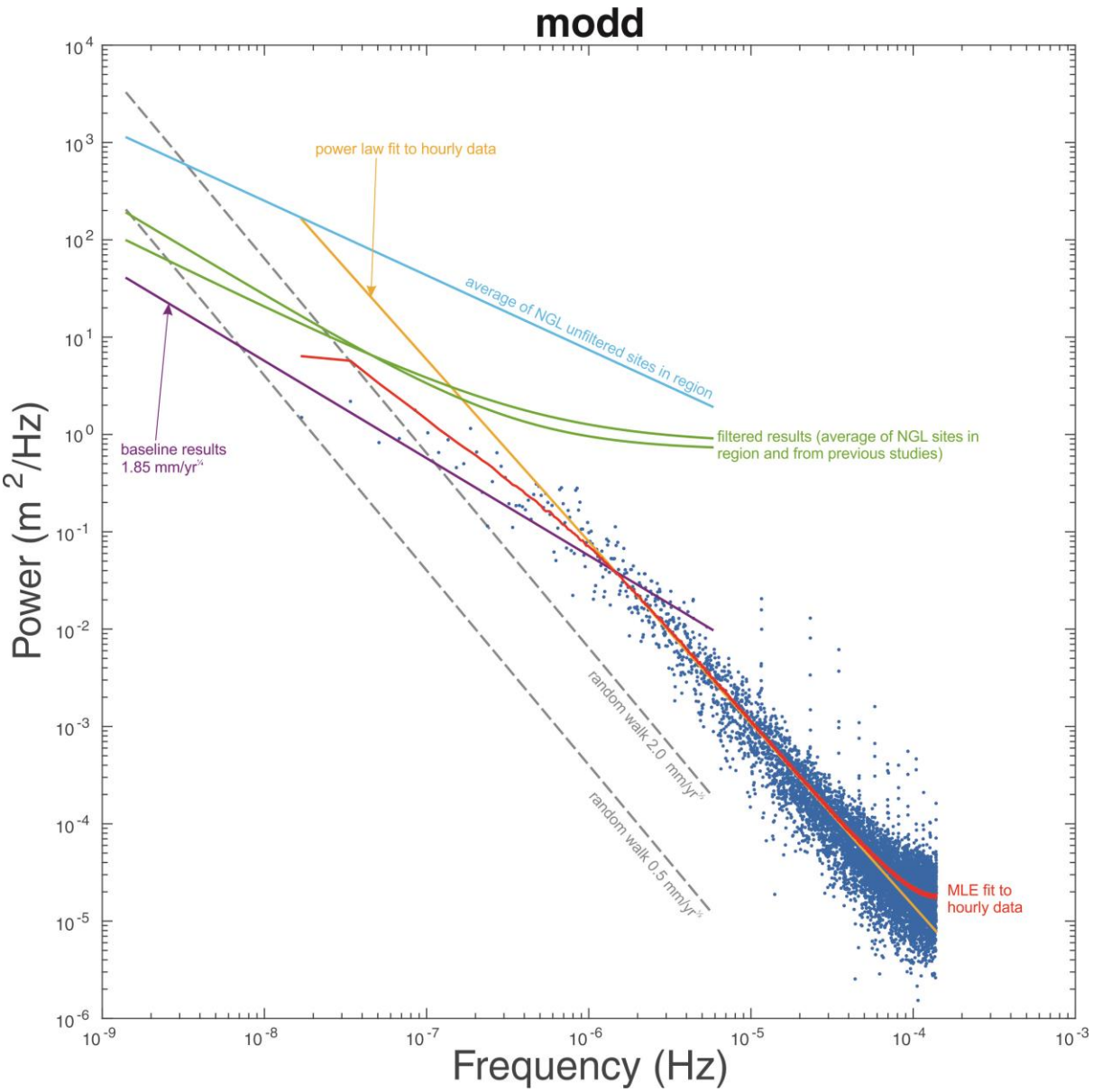

Figure 4c. Power Spectrum for site MODD (blue dots). Also included on the plot is the spectrum derived from the MLE analysis (below) and some representative spectra from the literature review and the NGL time series in the region.

Maximum Likelihood Analysis

As mentioned above there is a serious computational burden involved in MLE primarily centred on the covariance matrix, computing its inverse and its determinant and is one of the reasons for the development of heuristic methods. Even using daily observations (as opposed to hourly) a simple ML algorithm can take many hours per site depending on the length and complexity of the covariance model chosen. For sites such as AME1, ANJM and MODD with over 2800 days (68000+ hours) forming a covariance matrix alone would require around 35Gb of memory without attempting to invert it etc. Therefore attention must be placed on exactly how to process the data to get a satisfactory result within a reasonable amount of computational burden (in both time and size). Depending on the stochastic model chosen and whether the series is free from gaps and outliers certain methods allow various kinds of computational speed ups and the ability to forgo the creation

of a full covariance matrix. If we choose a stochastic model where the covariance matrix, or its cholesky decomposition, is Toeplitz then there are several methods that can be employed that can be of the $O(n^2)$ or even in some circumstances O(n log n) instead of the usual $O(n^3)$ in the number of computations required.

The first obvious choice is to convert the hourly data to daily data by simple averaging and then use conventional methods to calculate the stochastic noise parameters. We chose to use a power law plus white noise model and estimate a piece-wise linear trend with break points at the end of each year. The results are shown in Table 2.

Table 2. ML estimated parameters from daily averaged results assuming a power-law plus white noise model with a linear model that estimates a piece-wise linear trend with break points at the end of each year. The results do not differ significantly when a single trend is used instead. * these amplitudes have been multiplied by $\Delta t^{-\kappa/4}$ to compare with the amplitudes in Table 1. See Appendix A.

Site name	Spectral Index κ	Power Law Amplitude* (mm/yr$^{-\kappa/4}$)	White Noise Amplitude (mm)
0647	-1.95 ± 0.13	7.00 ± 0.31	0.00 ± 0.0010
AME1	-1.85 ± 0.04	4.71 ± 0.06	0.00 ± 0.0000
ANJM	-1.87 ± 0.04	5.21 ± 0.07	0.00 ± 0.0001
dw16	-2.15 ± 0.11	9.56 ± 0.35	0.00 ± 0.0007
dw26	-2.03 ± 0.11	7.94 ± 0.29	0.00 ± 0.0000
dzyl	-2.08 ± 0.15	8.65 ± 0.41	0.00 ± 0.0000
eems	-1.65 ± 0.14	4.29 ± 0.19	0.00 ± 0.0011
froo	-1.95 ± 0.14	6.10 ± 0.28	0.00 ± 0.0007
grij	-1.71 ± 0.14	5.07 ± 0.22	0.00 ± 0.0000
MODD	-1.86 ± 0.04	4.76 ± 0.06	0.00 ± 0.0001
norg	-1.94 ± 0.13	6.49 ± 0.29	0.00 ± 0.0009
over	-2.01 ± 0.14	6.80 ± 0.30	0.00 ± 0.0013
sted	-1.83 ± 0.17	5.88 ± 0.28	0.00 ± 0.0000
tenp	-1.89 ± 0.09	6.10 ± 0.18	0.00 ± 0.0000
tjuc	-1.80 ± 0.12	5.29 ± 0.24	0.00 ± 0.0015
usqu	-1.99 ± 0.15	7.35 ± 0.36	0.00 ± 0.0000
veen	-1.97 ± 0.09	7.32 ± 0.21	0.00 ± 0.0003
wsra	-2.21± 0.11	9.05 ± 0.30	0.00 ± 0.0000
zand	-2.00 ± 0.14	7.91 ± 0.35	0.00 ± 0.0019
zdvn	-2.03 ± 0.13	7.50 ± 0.34	0.00 ± 0.0010
zeer	-1.68 ± 0.15	4.41 ± 0.21	0.00 ± 0.0000
weighted mean	-1.90 ± 0.02	5.27 ± 0.22	0 ± 0

We find very consistent results for all the sites with the spectral index close to -1.90 ± 0.02, amplitude of 5.3 ± 0.2 mm/yr$^{-\kappa/4}$ and no white noise. This is inconsistent with previous studies for daily GPS and appears to reflect the noise at high frequency in the hourly data. For the three longest sites we can also analyse the time series averaged to three days and one week (Table 3). The main finding from this is a reduction of the spectral index as we average over longer time scales. This is consistent with the change in the slope in the power spectrum seen in Figures 3 and 4.

As mentioned above the computational burden to analyse the hourly data with a power-law plus white or a FIGGM plus white noise model would be too great. However two factors do allow us to perform an MLE on the data. First, Figures 3 and 4 and the white noise amplitudes in Tables 2 and 3, lead us to assume that we do not have a white noise component in the data (at least not at the level

measurable) and secondly the time series are very nearly completely continuous, that is, there are very few gaps in the data.

Table 3. ML estimated parameters for daily, tridaily and weekly averaged time series from the three longest sites. Results from a power-law plus white noise and an iGGM plus white noise model are shown. Cells where an uncertainty is not given are either because the uncertainty is smaller than the decimal places given or because no uncertainty was estimated

Site	Sampling	Model	κ_R	κ_L	γ	σ_{pl}*	σ_{wh}	trend
AME1	Daily	pl	-1.85 ± 0.04			0.308 ± 0.004	0.0	-6.97 ± 1.22
		figgm	-1.98 ± 0.01	-0.07 ± 0.00	0.926 ± 0.004	0.318 ± 0.0003	0.003 ± 0.0000	-6.59 ± 0.04
	Tri-daily	pl	-1.40			0.426 ± 0.010	0.000 ± 0.0000	-6.85 ± 0.25
		figgm	-2.00 ± 0.25	-0.85 ± 0.12	0.572 ± 0.110	0.421 ± 0.010	0.000 ± 0.0196	-6.70 ± 0.10
	Weekly	pl	-1.26			0.464 ± 0.0162	0.0	-6.81 ± 0.16
		figgm	-1.31 ± 0.12	-0.003 ± 1.17	0.975 ± 0.028	0.463 ± 0.0162	0.000 ± 0.056	-6.70 ± 0.12
ANJM	Daily	pl	-1.87 ± 0.04			0.332 ± 0.0044	0.000 ± 0.00	-3.79 ± 1.39
		figgm	-2.00 ± 0.01	-0.007	0.908	0.325 ± 0.0040	0.000 ± 0.000	-3.69 ± 0.03
	Tri-daily	pl	-1.23			0.447 ± 0.0102	0.000 ± 0.000	-3.78 ± 0.16
		figgm	-2.00 ± 0.27	-0.71 ± 0.10	0.516 ± 0.096	0.438 ± 0.0101	0.000 ± 0.000	-3.71 ± 0.06
	Weekly	pl	-0.99			0.472 ± 0.0165	0.000 ± 0.001	-3.76 ± 0.08
		figgm	-1.00 ± 0.09	-0.00 ± 0.01	0.989 ± 0.012	0.469 ± 0.0164	0.000 ± 0.035	-3.72 ± 0.08
MODD	Daily	pl	-1.86 ± 0.04			0.307 ± 0.0041	0.000 ± 0.00	-3.10 ± 1.27
		figgm	-1.70 ± 0.01	-0.01 ± 0.00	0.995 ± 0.003	0.330 ± 0.0008	0.000 ± 0.00	-3.02 ± 0.22
	Tri-daily	pl	-1.48			0.426 ± 0.0098	0.000 ± 0.00	-3.02 ± 0.32
		figgm	-1.48 ± 0.06	-0.00 ± 0.01	0.998 ± 0.002	0.425 ± 0.0097	0.000 ± 0.01	-3.08 ± 0.28
	Weekly	pl	-1.52			0.424 ± 0.0332	0.176 ± 0.05	-3.05 ± 0.29
		figgm	-1.49 ± 0.13	-0.00 ± 1.70	0.997 ± 0.004	0.435 ± 0.0545	0.160 ± 0.10	-3.09 ± 0.25

* Amplitudes are converted so they do not contain the Δt scaling (used in CATS) so that the PL and FIGGM results can be compared. See Appendix A.

All three long sites have only 19 or 20 out of over 60000+ hours missing[1] and so we can fill those gaps by linear interpolation without fear of that contaminating the results. Now because we are only assuming one noise model we can perform an MLE that is efficiently computed using the Fast Fourier transform in O(n log n) operations.

For the analysis of the hourly data we selected to use three linear models: trend only, piecewise linear trends with breakpoints at the end of each year and a trend plus acceleration (all models also include an annual and semi-annual signal). We also selected to test three stochastic models: power-law noise only, FIGGM only and white noise only (as a null hypothesis). The results are given in Tables 4, 5, and 6 below. The upper tables give the stochastic noise parameters and the lower give the estimates of the trends (and accelerations) and their uncertainties. The BIC for the most likely stochastic and linear model combination is highlighted in all the tables. In every case the preferred stochastic model is the FIGGM (which can be visually confirmed in Figure 4). The preferred linear model is the trend only for AME1 and the trend plus acceleration for ANJM and MODD; but only slightly for ANJM compared to the trend only. We see that in the case of the FIGGM model that the κ_R parameter is fairly consistent throughout whereas the κ_L and γ parameters are dependent on the linear model and reflect the conflict between the stochastic and linear parameters. For instance in the case of MODD, where there is an obvious long period variation, the κ_L parameter which characterises the power spectrum at low frequencies changes from -1.20 for the trend only to -0.30 and γ, which represents the

[1] Although it is obvious that where some data is lost over a few hours the coordinates are generated with the same coordinate as prior to the data loss.

cross-over frequency, increases indicating a shift to lower frequencies. The piecewise linear trend "soaks up" some of the low frequency power and the stochastic model becomes less correlated.

Table 4: AME1

	Linear Model	κ_R	κ_L	γ	σ	MLE	BIC
FIGGM Noise	Trend	-1.90	-0.91	0.9847	0.095538	538311.421	**-1076511.469**
	Piecewise	-1.89	-0.28	0.9912	0.095511	538330.531	-1076471.728
	Acceleration	-1.89	-0.91	0.9848	0.095538	538311.450	-1076500.389
Power-Law Noise	Trend	-1.87	-	-	0.095653	538228.208	-1076367.318
	Piecewise	-1.87	-	-	0.095653	538228.567	-1076290.074
White Noise	Trend	-	-	-	0.834429	389448.878	-778819.794
	Piecewise	-	-	-	0.646531	406973.038	-813790.154

		Stochastic Model				
	Year	FIGGM	FIGGM*	FIGGM†	Power Law	White
Piecewise Linear Trends	2007	-7.48 ± 0.25	-7.53 ± 0.60	-7.53 ± 0.60	-8.20 ± 5.03	-7.75 ± 0.02
	2008	-6.87 ± 0.31	-6.81 ± 0.72	-6.81 ± 0.72	-6.03 ± 5.05	-6.82 ± 0.01
	2009	-6.96 ± 0.31	-6.99 ± 0.72	-6.99 ± 0.72	-7.22 ± 5.07	-6.96 ± 0.01
	2010	-6.06 ± 0.31	-5.98 ± 0.72	-5.98 ± 0.72	-5.51 ± 5.07	-6.08 ± 0.01
	2011	-6.60 ± 0.31	-6.64 ± 0.72	-6.64 ± 0.72	-6.38 ± 5.05	-6.60 ± 0.01
	2012	-5.97 ± 0.31	-6.02 ± 0.72	-6.02 ± 0.72	-7.32 ± 5.05	-5.95 ± 0.01
	2013	-6.02 ± 0.32	-5.99 ± 0.73	-5.99 ± 0.73	-5.54 ± 5.07	-6.06 ± 0.02
	2014	-10.22 ± 0.47	-10.40 ± 0.94	-10.40 ± 0.94	-10.89 ± 5.67	-10.06 ± 0.02
Trend Only			-6.76 ± 0.08	-6.75 ± 0.08	-7.00 ± 1.58	-6.58 ± 0.0014
Trend plus Acceleration	Trend			-6.80 ± 0.24		
	Acc.			0.0160 ± 0.06		

* This uses the stochastic parameters derived from the single trend only model, † uses the stochastic parameters from the trend and acceleration model

The crucial parameters in this model are κ_L and γ as these really dictate the uncertainty estimates of the trends (see the bottom half of Tables 4, 5 and 6). We notice that these parameters are most consistent when we look at the preferred model based on the BIC. To test this further we simulated 400 time series using the stochastic and linear parameters from MODD for the trend plus acceleration model. We then fit those parameters using MLE for all three linear models. The results, in the form of histograms, are shown in Figure 5. We can see that the estimated stochastic parameters for the trend and piecewise continuous are all within the expected ranges from the simulations including the -1.2 and -0.3 for κ_L.

The bottom halves of Tables 4, 5 and 6 show the estimated trends (and accelerations) and their uncertainties as a function of the stochastic model used. We can immediately see the overly pessimistic and overly optimistic uncertainties from the power-law and the white noise model; there is a scaling factor of 250-500 between the uncertainties of the two models. The two FIGGM columns marked with a * and a † take the stochastic model parameters from the trend only and the trend plus acceleration models and apply it to the piecewise linear model. For the two sites where the trend plus acceleration model is the most likely we see the uncertainties from that model are somewhere between the other two. For AME1 where there is no acceleration, the uncertainties are close to the trend only model but bigger than the piecewise linear model which probably under predicts the uncertainties.

Table 5: ANJM

	Linear Model	κ_R	κ_L	γ	σ	MLE	BIC
FIGGM Noise	Trend	-1.90	-0.81	0.9839	0.098739	536047.484	-1071983.595
	Piecewise	-1.93	-0.10	0.9904	0.098703	536072.260	-1071955.186
	Acceleration	-1.93	-0.66	0.9859	0.098731	536053.307	**-1071984.104**
Power-Law Noise	Trend	-1.90	-	-	0.098896	535938.434	-1071787.769
	Piecewise	-1.90	-	-	0.098896	535938.535	-1071710.011
White Noise	Trend	-	-	-	0.796477	392646.309	-785214.656
	Piecewise	-	-	-	0.633136	408411.147	-816666.371

	Stochastic Model					
	Year	FIGGM	FIGGM*	FIGGM†	Power Law	White
Piecewise Linear Trend	2007	-5.18 ± 0.20	-5.22 ± 0.52	-5.22 ± 0.41	-4.75 ± 5.90	-4.61 ± 0.02
	2008	-2.70 ± 0.23	-2.74 ± 0.62	-2.73 ± 0.50	-3.31 ± 5.91	-2.84 ± 0.01
	2009	-5.31 ± 0.23	-5.28 ± 0.62	-5.29 ± 0.50	-4.78 ± 5.94	-5.27 ± 0.01
	2010	-3.70 ± 0.23	-3.72 ± 0.63	-3.72 ± 0.50	-3.61 ± 5.93	-3.70 ± 0.01
	2011	-2.79 ± 0.23	-2.73 ± 0.63	-2.75 ± 0.50	-2.07 ± 5.91	-2.79 ± 0.01
	2012	-3.46 ± 0.23	-3.60 ± 0.63	-3.56 ± 0.50	-5.00 ± 5.91	-3.45 ± 0.01
	2013	-3.37 ± 0.24	-3.29 ± 0.64	-3.32 ± 0.51	-2.90 ± 5.94	-3.37 ± 0.01
	2014	-4.54 ± 0.37	-4.56 ± 0.84	-4.57 ± 0.69	-4.27 ± 6.62	-4.61 ± 0.02
Trend Only	Trend		-3.85 ± 0.06	-3.84 ± 0.04	-3.82 ± 1.91	-3.68 ± 0.0013
Trend Plus Acceleration	Trend			-4.41 ± 0.14		
	Acc.			0.1625 ± 0.04		

* This uses the stochastic parameters derived from the single trend only model, † uses the stochastic parameters from the trend and acceleration model

Table 6: MODD

	Linear Model	κ_R	κ_L	γ	σ	MLE	BIC
FIGGM Noise	Trend	-1.90	-1.20	0.9774	0.096103	537906.205	-1075701.037
	Years	-1.90	-0.30	0.9907	0.096054	537941.284	-1075693.233
	Acceleration	-1.90	-0.65	0.9876	0.095697	538197.075	**-1076271.640**
Power-Law Noise	Trend	-1.87	-	-	0.096204	537833.798	-1075578.497
	Years	-1.87	-	-	0.096204	537834.331	-1075501.601
White Noise	Trend	-	-	-	1.508738	348766.276	-697454.591
	Years	-	-	-	0.645565	407075.688	-813995.454

		Stochastic Model				
	Year	FIGGM	FIGGM*	FIGGM†	Power Law	White
Piecewise Linear Trend	2007	-1.66 ± 0.25	-1.77 ± 1.02	-1.68 ± 0.39	-2.33 ± 5.13	-1.67 ± 0.02
	2008	-0.76 ± 0.31	-0.78 ± 1.14	-0.76 ± 0.48	-0.56 ± 5.15	-0.75 ± 0.01
	2009	-3.22 ± 0.31	-3.16 ± 1.14	-3.21 ± 0.48	-2.77 ± 5.17	-3.21 ± 0.01
	2010	-2.19 ± 0.31	-2.02 ± 1.15	-2.13 ± 0.48	-1.74 ± 5.17	-2.22 ± 0.01
	2011	-2.88 ± 0.31	-2.99 ± 1.15	-2.93 ±0.48	-2.60 ± 5.15	-2.85 ± 0.01
	2012	-4.31 ± 0.31	-4.37 ± 1.15	-4.31 ± 0.48	-5.45 ± 5.15	-4.31 ± 0.01
	2013	-4.15 ± 0.32	-3.93 ± 1.16	-4.08 ± 0.49	-3.02 ± 5.17	-4.20 ± 0.02
	2014	-6.31 ± 0.46	-6.82 ± 1.42	-6.50 ± 0.67	-7.12 ± 5.78	-6.16 ± 0.02
Trend Only	Trend		-2.88 ± 0.17	-2.74 ± 0.04	-3.08 ± 1.62	-2.97 ± 0.0026
Trend Plus Acceleration	Trend			-0.75 ± 0.14		
	Acc.			-0.5801 ± 0.04		

* This uses the stochastic parameters derived from the single trend only model, † uses the stochastic parameters from the trend and acceleration model

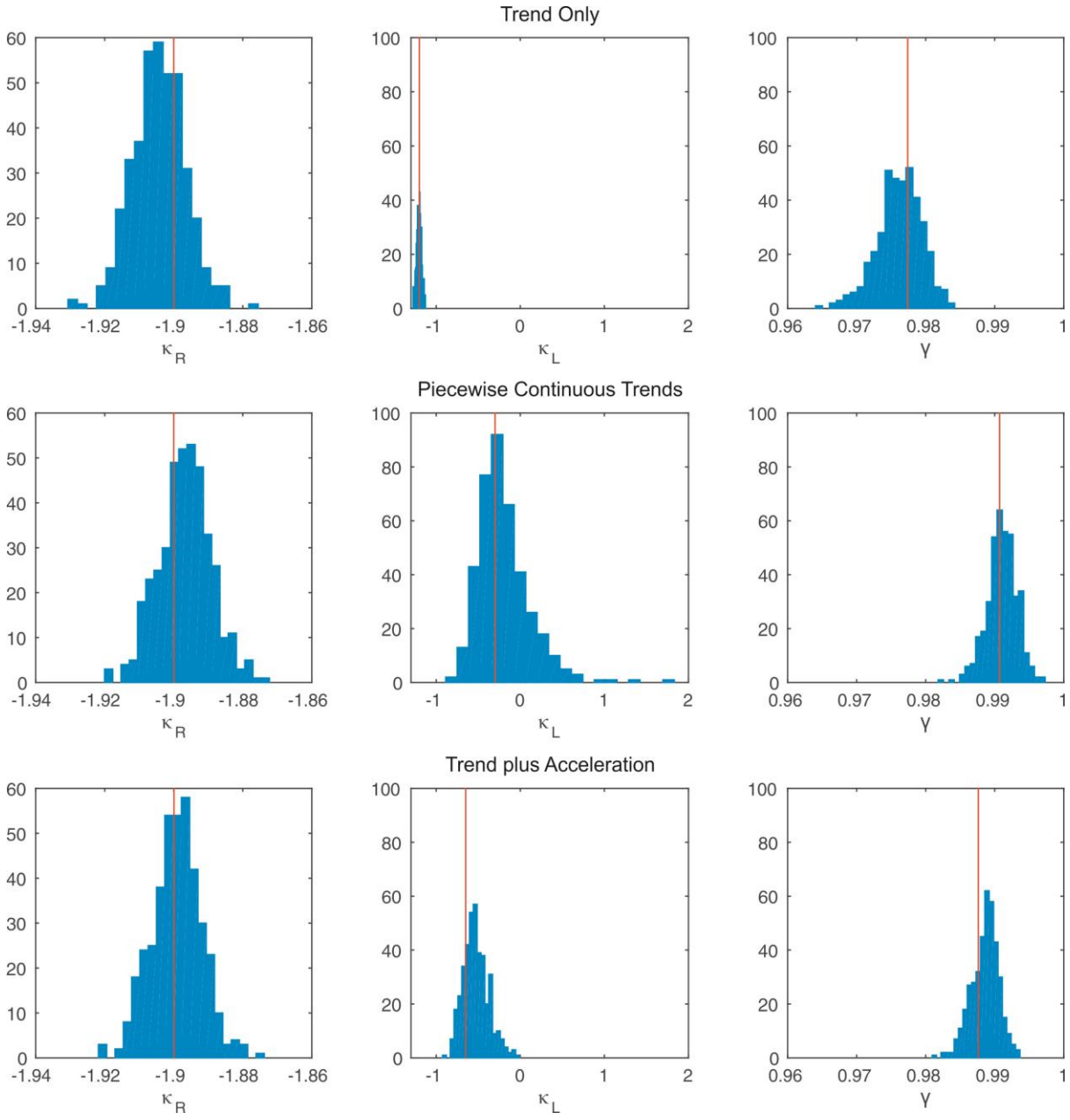

Figure 5. Histograms of the estimated parameters from 400 Monte Carlo simulations of the MODD time series (based on the trend plus acceleration model). The red lines indicate the estimated parameters from the actual time series.

Given a realistic stochastic model we can use this to check for any significant time-dependent changes. Site AME1 is a good example. We can see from Table 4 that 2014 has a trend that is around 3-4 mm/yr larger than the other years. Is this significant or are the variations in the trend expected from the stochastic model? We can ask whether the yearly trends are significantly different from the single trend only but have to be cautious because we are estimating two sets of parameters from a single dataset so they are correlated to some extent. Taking cross-correlations into account and propagating the covariances correctly we find that 2014 is indeed significantly different from the long

term trend (Figure 6). However this is based on the general 06-GPS/NAM model and not modified to align it to the filtered regional results.

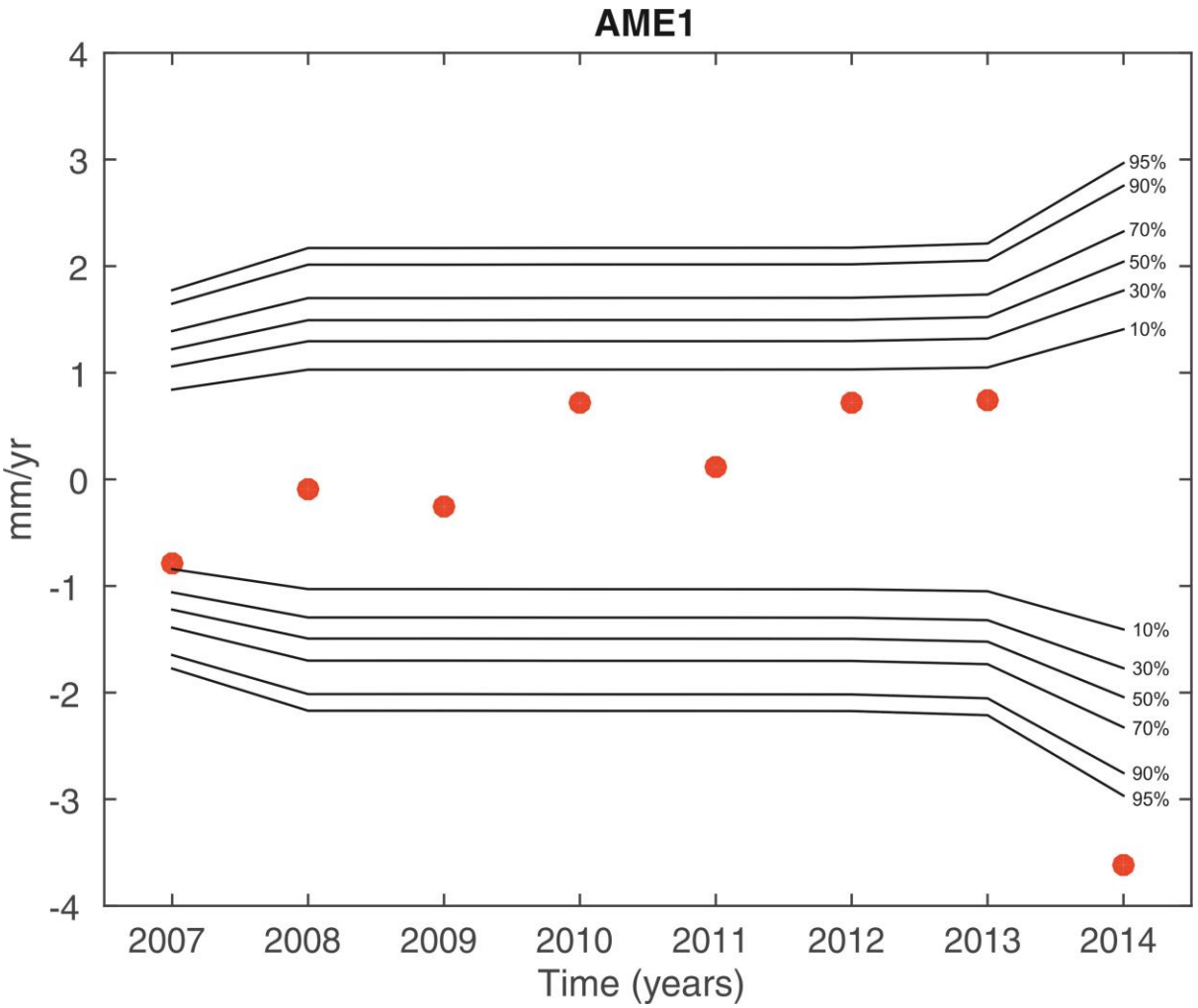

Figure 6. Significance of the piecewise linear trends with respect to the long-term trend given the optimal stochastic model for the data. Red dots are the estimated yearly trends with respect to the long-term trend. Black lines indicate the confidence bounds. The bounds appear much larger than the individual formal errors because we have 8 degrees of freedom rather than typically examining the one-dimensional confidence. **NOTE : this is purely from the optimal stochastic model derived from the data no attempt has been made to account for systematic effects or align the noise model with previous findings and processing results.**

Comparison with Leica CrossCheck Time Series

We were also supplied with the two years of AME1, ANJM and MODD processed using the Leica CrossCheck service which uses the Bernese software. In a similar manner to the report "Crosschecking the GPS Leica CrossCheck service" we examined the baseline differences between AME1 and ANJM with respect to MODD. We have plotted the power spectra in Figure 7 together with the power spectra from the same baselines from the 06-GPS results and also plotted the average spectrum calculated from the filtered NGL time series.

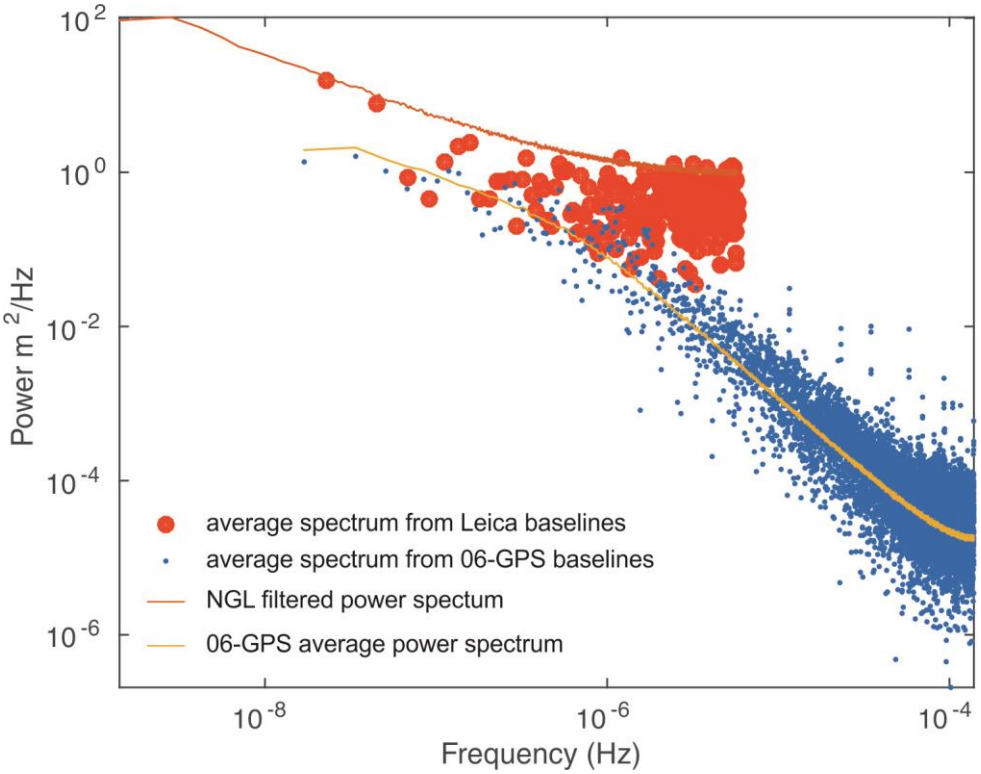

Figure 7. Power Spectra for the Bernese derived Leica time series baselines and the 06-GPS baselines AME1-MODD and ANJM-MODD. Red dots are the average spectra from the two Leica baseline time series, blue dots from the 06-GPS data. Orange line shows the average spectrum from the NGL filtered series and the yellow line represents the average spectrum from the 06-GPS data.

The results show that the Leica baseline results are less noisy than the filtered NGL series and slightly more noisy that the 06-GPS results. The ML analyses of the baselines give a spectral index of -0.85 and -0.86 for AME1-MODD and ANJM-MODD respectively with amplitudes of 2.43 ± 0.38 and 2.10 ± 0.31. The estimated white noise amplitudes were 1.56 ± 0.07 and 1.29 ± 0.06 mm. For comparison the average values from the filtered NGL results are a spectral index of -0.85 with amplitude of 5.26 ± 0.17 and white noise amplitude of 2.14 ± 0.11 mm.

Discussion

The analysis of the three long permanent sites together with the shorter series indicates a consistent FIGGM model with κ_R being just short of random walk at -1.9. γ is around 0.98 which equates to a cross over period of around 10+ days and the spectral index at low frequency, κ_L, is just below flicker noise and in the range [-0.65,-0.91]. The spectral index at low frequency is certainly consistent with the other time series produced by various groups and with the results from the literature review. However the amplitude is smaller than both the unfiltered and filtered series and the Leica baseline series and is similar to the results from short baseline studies. It is very hard to reconcile that the noise is equivalent to short baseline processing given that many errors are differenced to negligible levels in those studies, something that cannot be achieved over the much wider area of the network. It seems likely that the processing methodology used constrains the positions to the extent that some real land motion could be suppressed particularly at high frequencies. Flicker noise has been shown to characterise the spectrum at high frequencies (up to 1Hz) [*Bock et al.*, 2000; *J. Langbein and Bock*, 2004] whereas a spectral index close to -2 is a likely outcome of a Kalman filter that probably treats the coordinates in

the constraint as a random walk. How much the low frequency end of the spectrum is constrained, and therefore effecting any estimates of subsidence or changes in subsidence, is unknown. Comparisons with the Leica CrossCheck results suggest that it isn't biased by any significant amount but the test is very limited. To err on the side of caution in our results and conclusions we recommend aligning the noise model with previous findings.

Stochastic Model for the Vertical Continuous Data

The results from the three long time series are seen to be sufficiently similar to derive a single noise model for all of the continuous data. This model, which we will call the 06-GPS/NAM model, is a FIGGM with parameters that are averages from the three models with the lowest BIC. The parameters for κ_R, κ_L, γ are -1.91, -0.74, 0.9861 respectively with σ = 0.0967 mm. This model gives an uncertainty in the trend of 0.6 mm/yr after 1 year down to 0.04 mm/yr after 10 years. However, given the uncertainty in the processing method and the comparison with both the results from the literature review and the other groups time series we will present some alternative models to consider:

1. General 06-GPS/NAM model : [κ_R = -1.91, κ_L = -0.74, γ = 0.9861, σ = 0.0967]
2. General 06-GPS/NAM model plus 0.5 mm/√yr of random walk. There is the possibility that there exists a random walk due to monument instability that is not yet identifiable in the time series but will already influence the long term trend uncertainties. The magnitude reflects the estimate given by [*M A King and Williams*, 2009].
3. As for model 2 but 1 mm/√yr of random walk. As well as monument instability the random walk could be used to also reflect any long term variations that have been damped by the Kalman filter.
4. General 06-GPS/NAM model scaled by a factor of 3. This brings the power spectrum in line with the noise levels of the regionally filtered GPS data. However the power at high frequencies is too large – the power at high frequencies is tightly constrained (see Table 2)
5. 06-GPS/NAM modified at low frequencies to mimic the amplitude of the regional noise. The new parameters being [κ_R = -1.91, κ_L = -0.8525, γ = 0.99238, σ = 0.0967]. The main change is the parameter γ, which shifts the cross over frequency to a lower value which then increases the power at low frequencies. This is purely a back of the envelope calculation to mimic the regional noise and has no physical reason for the change in parameters.
6. General 06-GPS/NAM model with an additional FIGGM [κ_R = -2, κ_L = -0.8525, γ = 0.99806, σ = 0.04] to mimic the regional noise. This is similar to the argument for additional random walk so that only powers at low frequencies are affected except the spectrum will tend to -0.8525 instead of -2 at very low frequencies.
7. A model based on the daily solutions from the regional filtered data from NGL. This model is a power law with spectral index = -0.8525 and amplitude of 1.50 mm (5.26 mm/yr$^{\kappa/4}$ in CATS notation) and white noise of amplitude 2.13 mm.

Examples of simulated time series from the 7 models together with the detrended AME1 series are plotted in Figure 8.

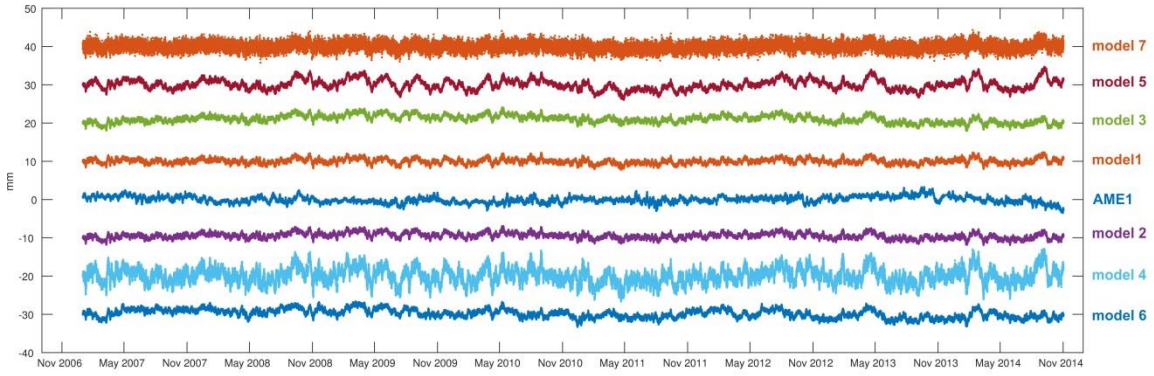

Figure 8. Examples of simulated time series from the 7 models described in the text. Also shown for comparison is the detrended time series for AME1.

We can see that some of the models look very similar visually to AME1 except models 4, 7 and partially 5. Model 7 is to be expected since it is projecting the results from a daily solution down to hourly values and therefore has too much power at these frequencies (although this is not important when estimating the trend uncertainties). The power-spectrum of these models is shown in Figure 9.

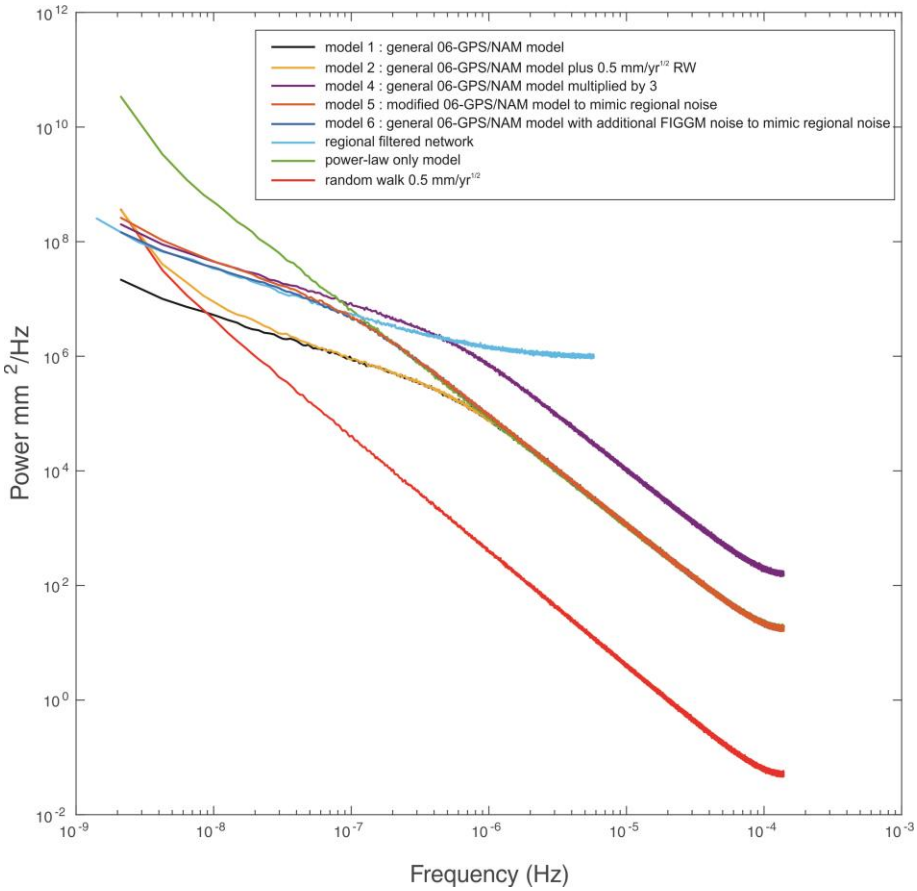

Figure 9. Power Spectra of the six of the proposed models (model 3 not shown).

We can see that the two models where the 06-GPS/NAM model is modified to mimic the regional noise at low frequencies do just that whilst they retain the correct power at low frequencies. Model 4 which simply scales the 06-GPS model by 3 is not a reflection of the hourly data at high frequencies.

Finally the uncertainties in the trends as a function of the length of the time series is plotted in Figure 10 and shown (per year) in Table 7.

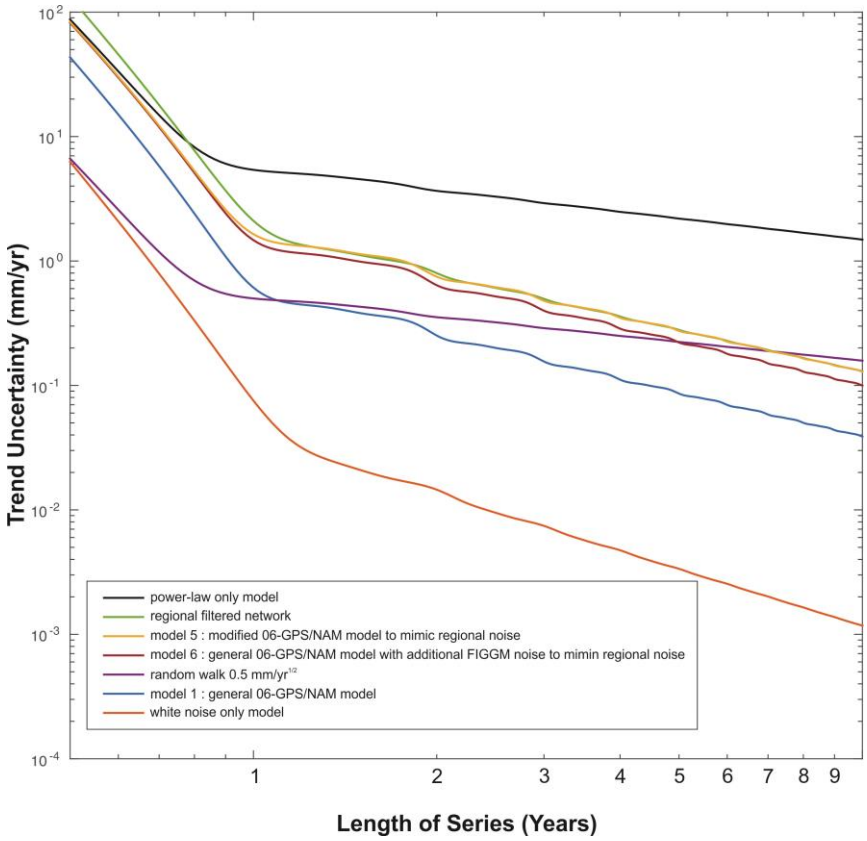

Figure 10. Trend Uncertainties in mm/yr for the various stochastic models as a function of the length of time of the series assuming hourly data. The small wiggles and the change in slope below one year are a result of estimating the annual and semi-annual signal simultaneously with the trend and intercept.

Table 7. Trend Uncertainties for the various stochastic models as a function of the length of the time series

Number of Years	Trend Uncertainty (mm/yr)						
	Model 1	Model 2	Model 3	Model 4	Model 5	Model 6	Model 7
1	0.61	0.79	1.17	1.82	1.63	1.22	2.08
2	0.25	0.43	0.75	0.75	0.75	0.57	0.80
3	0.16	0.33	0.60	0.47	0.48	0.37	0.50
4	0.11	0.27	0.51	0.33	0.35	0.27	0.36
5	0.09	0.24	0.46	0.26	0.27	0.21	0.28
6	0.07	0.22	0.41	0.21	0.22	0.17	0.23
7	0.06	0.20	0.38	0.18	0.19	0.15	0.19
8	0.05	0.18	0.36	0.15	0.16	0.13	0.17
9	0.04	0.17	0.34	0.13	0.14	0.11	0.15
10	0.04	0.16	0.32	0.12	0.13	0.10	0.13
11	0.03	0.15	0.30	0.10	0.12	0.09	0.12
12	0.03	0.15	0.29	0.09	0.11	0.08	0.11
13	0.03	0.14	0.28	0.09	0.10	0.08	0.10
14	0.03	0.14	0.27	0.08	0.09	0.07	0.09

Model 1: general 06-GPS/NAM model
Model 2: general 06-GPS/NAM model plus 0.5 mm/√yr random walk
Model 3: general 06-GPS/NAM model plus 1 mm/√yr random walk
Model 4: general 06-GPS/NAM model multiplied by 3
Model 5: modified 06-GPS/NAM model to mimic regional noise
Model 6: general 06-GPS/NAM model with additional FIGGM noise to mimic regional noise
Model 7: regional noise (daily solution)

We can see from Figure 10 that the choice of stochastic model affects the decay rate of the trend uncertainty. Random walk has a slower decay rate than flicker noise and white noise and would dominate the trend uncertainty at around 5 or more years despite not being visible in the power spectrum until after 10+ years (and probably much longer [*Johnson and Agnew*, 2000]). Both of the modified 06-GPS models (5 and 6) mimic the behaviour of the regional models both in terms of power spectrum and trend uncertainty. However, as stated above, model #5 visually does not look as similar to the real data, so the preferred model is #6 which provides a good compromise between the base 06-GPS/NAM model derived from the data and typical uncertainties found for regionally filtered GPS datasets and baseline solutions. At 1 year the trend uncertainty is 1.2 mm/yr and is around twice that of model 1 whereas after 14 years the uncertainty is 0.1 mm/yr which is around 3 times the uncertainty derived from model 1. An alternative solution would be Model 2; the combination of the 06-GPS/NAM model and random walk of 0.5 mm/√yr which has a more sound physical basis.

Stochastic Model for the Horizontal Continuous Data

Whilst we have concentrated on the vertical time series we also need to apply the same methodology to the horizontal components. There is no reason to assume that the two horizontal components should behave in a different way stochastically (although there is some evidence that the east is slightly noisier than the north) so we will proceed to form one model for the horizontal. It is evident, particularly for ANJM in the north component that there are offsets on or around May 3rd 2009 and Feb 20th 2014 (see Figure 11). The offset in 2009 relates to the change in the reference station coordinates of stations 0687 and DRAC. The offset in 2014 may be related to the installation of several new stations at that time starting with Grijpskerk on 13th Feb, Norg on the 19th Feb and Eemskanaal on 20th Feb.

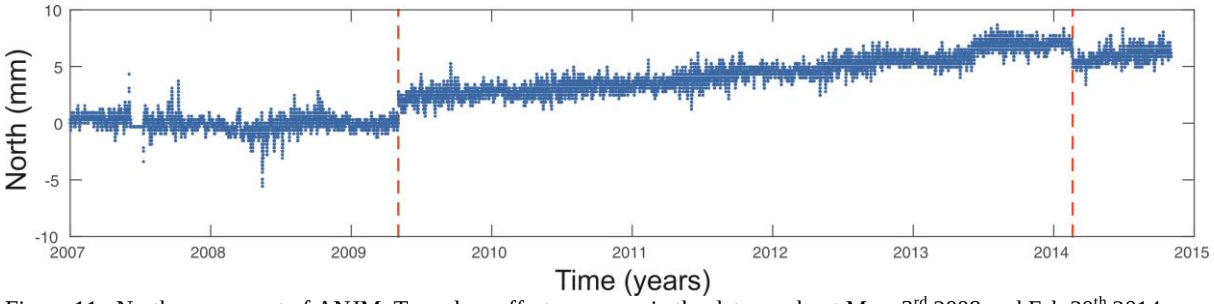

Figure 11. North component of ANJM. Two clear offsets are seen in the data on about May 3rd 2009 and Feb 20th 2014.

For ANJM in particular there also appears to be a change in trend at these dates. Therefore we use four linear models when estimating the stochastic noise parameters. The first model is a linear trend together with annual and semi-annual signals and the two offsets. Model 2 also includes an acceleration term. Model 3 is a piecewise linear trend (as for the vertical) together with the annual, semi-annual and offsets and Model 4 incorporates 3 separate trends for each segment separated by an offset (together with the annual, semi-annual and the offsets themselves). The results of the stochastic model estimation is given in Table 8 below with the best choice for each based on the BIC.

Table 8. Estimated Noise Parameters for the Horizontal Components.
Highlighted BIC's are the preferred models

	κ_R	κ_L	γ	σ	BIC
AME1 North					
Model 1 :	-1.72	-0.82	0.9258	0.1518	-63947.549
Model 2 :	-1.72	-0.79	0.9288	0.1518	-63949.841
Model 3 :	-1.71	-0.53	0.9485	0.1517	**-63952.311**
Model 4 :	-1.72	-0.76	0.9318	0.1517	-63950.067
AME1 East					
Model 1 :	-1.99	-0.77	0.9033	0.1406	-74495.059
Model 2 :	-1.99	-0.71	0.9096	0.1405	**-74506.363**
Model 3 :	-1.99	-0.68	0.9129	0.1405	-74449.113
Model 4 :	-1.99	-0.71	0.9098	0.1405	-74495.568
ANJM North					
	κ_R	κ_L	γ	σ	BIC
Model 1 :	-1.76	-0.81	0.9490	0.1587	-57815.001
Model 2 :	-1.76	-0.78	0.9503	0.1587	-57807.618
Model 3 :	-1.76	-0.44	0.9633	0.1586	-57825.662
Model 4 :	-1.76	-0.66	0.9553	0.1587	**-57827.545**
ANJM East					
Model 1 :	-2.12	-0.76	0.8784	0.1290	**-86280.730**
Model 2 :	-2.12	-0.76	0.8784	0.1290	-86269.869
Model 3 :	-2.12	-0.68	0.8869	0.1290	-86244.354
Model 4 :	-2.12	-0.76	0.8788	0.1290	-86261.303
MODD North					
	κ_R	κ_L	γ	σ	BIC
Model 1 :	-1.86	-0.88	0.8885	0.1726	-46281.191
Model 2 :	-1.86	-0.87	0.8907	0.1726	-46281.308
Model 3 :	-1.85	-0.77	0.9039	0.1725	-46250.822
Model 4 :	-1.86	-0.82	0.8973	0.1726	**-46286.665**
MODD East					
Model 1 :	-2.00	-0.83	0.8801	0.1364	-78632.697
Model 2 :	-1.99	-0.72	0.8928	0.1363	**-78670.106**
Model 3 :	-1.99	-0.67	0.8982	0.1363	-78622.431
Model 4 :	-1.99	-0.75	0.8895	0.1363	-78649.470

Model 1 : Linear term, annual and semi-annual plus two visible offsets relating to updates of the reference station coordinates
Model 2: As for 1 together with an acceleration term
Model 3 : Piecewise linear trends for each year, annual, semi-annual and two offsets as for model 1.
Model 4 : As for model 1 but 3 trends relating to the segments formed by the offsets

The results from the three long time series are again seen to be sufficiently similar to derive a single noise model for all of the continuous data. This 06-GPS/NAM model is a FIGGM with parameters that are averages from the six models (two per site) with the lowest BIC. The parameters for κ_R, κ_L, γ are -1.91, -0.70, 0.9137 respectively with σ = 0.1481 mm. This is similar to the vertical component except for γ which is lower (such that the cross-over frequency is higher) and a σ that is higher. However despite σ being larger than the vertical the power at low frequencies is smaller. This model

gives an uncertainty in the trend of 0.3 mm/yr after 1 year down to 0.02 mm/yr after 10 years. However, as for the vertical, given the uncertainty in the processing method and the comparison with both the results from the literature review and the other groups time series we will present some alternative models to consider:

1. General 06-GPS/NAM model : [κ_R = -1.91, κ_L = -0.70, γ = 0.9137, σ = 0.1481]
2. 06-GPS/NAM modified at low frequencies to mimic the amplitude of the regional noise. The new parameters being [κ_R = -1.91, κ_L = -0.8281, γ = 0.9771, σ = 0.1481]. The main change is the parameter γ, which shifts the cross over frequency to a lower value which then increases the power at low frequencies. This is purely a back of the envelope calculation to mimic the regional noise and has no physical reason for the change in parameters.
3. General 06-GPS/NAM model with an additional FIGGM [κ_R = -2, κ_L = -0.8281, γ = 0.992, σ = 0.06] to mimic the regional noise.
4. A model based on the daily solutions from the regional filtered data from NGL. This model is a power law with spectral index = -0.8281 and amplitude of 0.76 mm (2.58 mm/yr$^{\kappa/4}$ in CATS notation) and white noise of amplitude 0.63 mm.

We have not included the models with random walk or the model that scaled the general 06-GPS/NAM model by 3. Figure 12 shows the fitted power spectra for the 3 long series (both north and east)

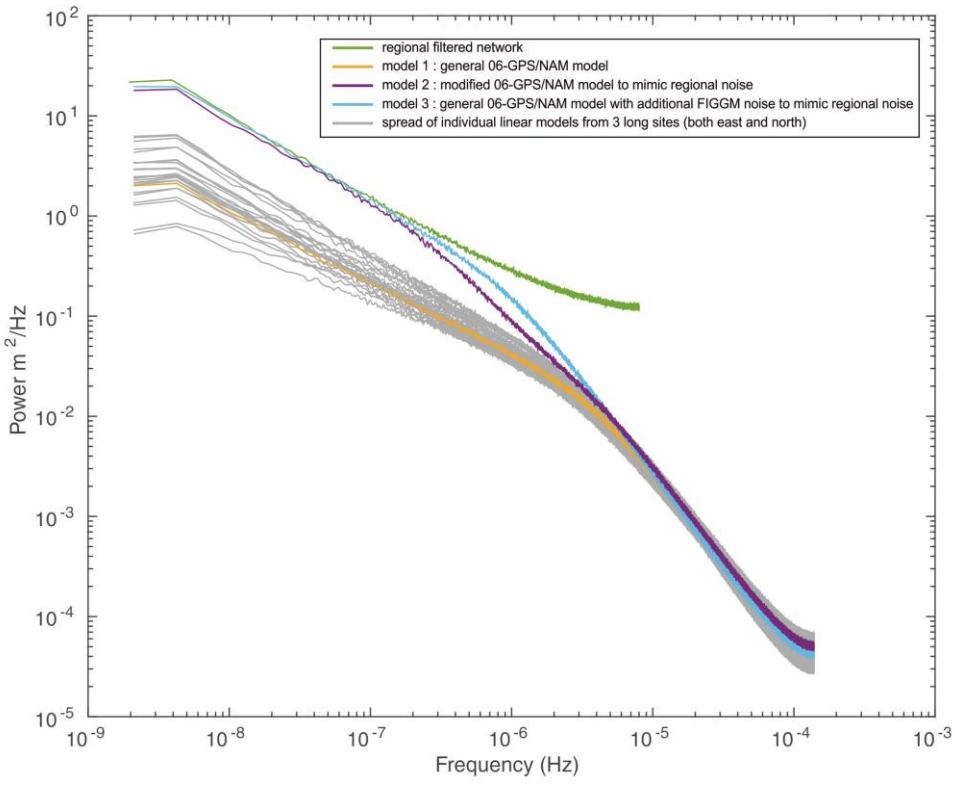

Figure 12. Fitted power spectra (derived from MLE) for AME1, ANJM and MODD in both components (grey). The coloured lines represent the various models given above.

Spatial Correlation in the Continuous Time Series

The reduction in time-correlated noise from unfiltered, to filtered, to small baseline solutions suggests that some of the noise is spatially correlated [*A Amiri-Simkooei*, 2009; *S.D.P. Williams et al.*, 2004]. [*S.D.P. Williams et al.*, 2004] speculated that if the time and spatial correlations are orthogonal to one another then the two effects can be treated separately and combined at the end. This was proven by [*A Amiri-Simkooei*, 2009] who summarized this by stating that the correlations between time series propagate directly into the correlation between parameters. Therefore the time series can be treated individually and their correlations can be added directly to create a covariance matrix of site velocities.

We have taken the time series for all continuous sites and, after removing the linear model, calculated the correlations between each site for the north, east and vertical components individually (correlations between components is generally considered to be minimal). The results are shown in Figure 13 along with a simple model of an exponential decay of the form

$$c = e^{-\rho x} \tag{10}$$

where c is the correlation, ρ is the decay parameter and x is the distance between two sites. The parameter ρ is estimated to be 0.0827, 0.1291 and 0.0887 for the north, east and vertical respectively. The correlation is strongest in the vertical and weakest in the east.

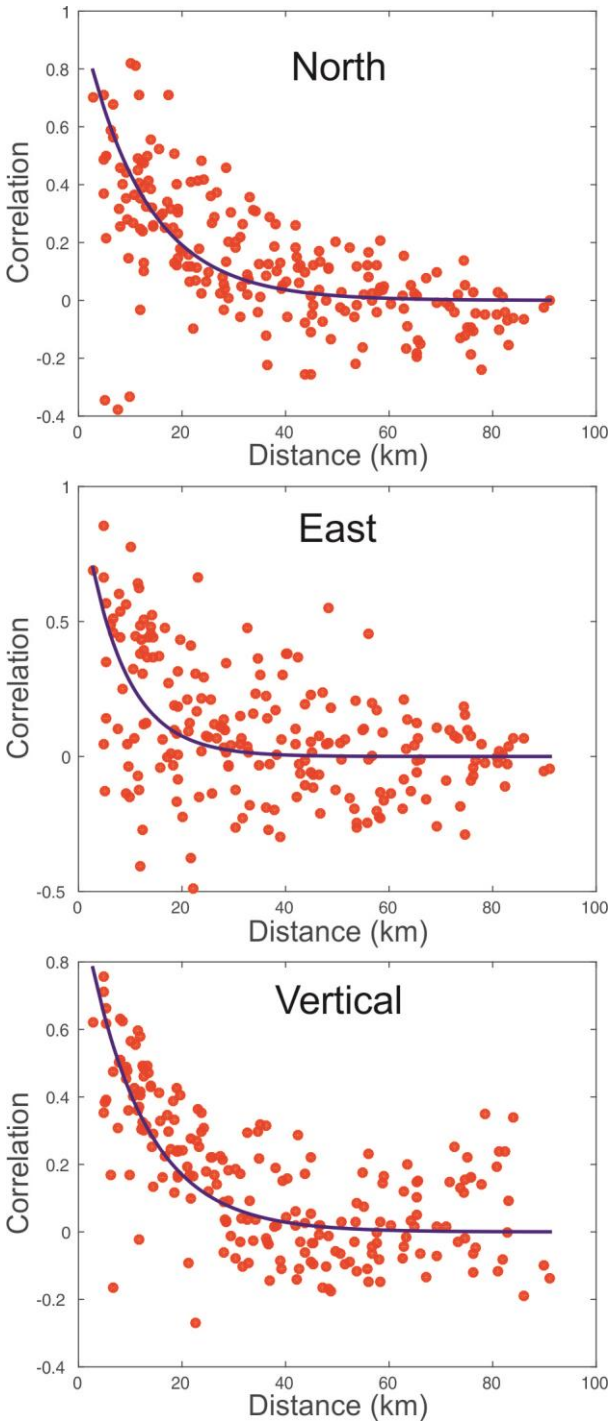

Figure 13. Correlations between the continuous GPS time series in the North, East and Vertical components. Blue line is the fitted exponential decay to the results.

Stochastic Model for the Campaign Data[i]

As discussed in the literature review there is very little understanding of uncertainties in campaign GPS. Presumably there is no difference in the systematic noise between campaign and continuous GPS so we should adopt the same models as for the continuous data and treat the campaign as a continuous series with many large gaps. The campaign data is also given as a single coordinate per campaign so we should derive a covariance matrix that is an average over the number of days of

measurement. The campaign data should presumably also suffer from a "set up" error every time the GPS equipment is installed. This is effectively an additional white noise to add to the covariance matrix derived above. The unknown in this is simply the amplitude of the noise. We know this is likely to be on the order of a few mm and we can use the results themselves to give us an estimate. Figure 14 below shows the height time series for the campaign sites that have had 4 or more measurements plotted along with a simulated noise equivalent to the modified 06-GPS/NAM model (#6) for the continuous data added to the trend calculated from the campaign data. We note that the scatter is not much different compared to the continuous data. The expected standard deviation for the campaign data from the continuous model is 1.1 ± 0.4 mm and the standard deviation of the 14 sites is 1.0 mm. Note we removed the results from the 2006 campaign for sites with the naming pattern M??? due to suspected initial settlement of newly installed benchmarks.

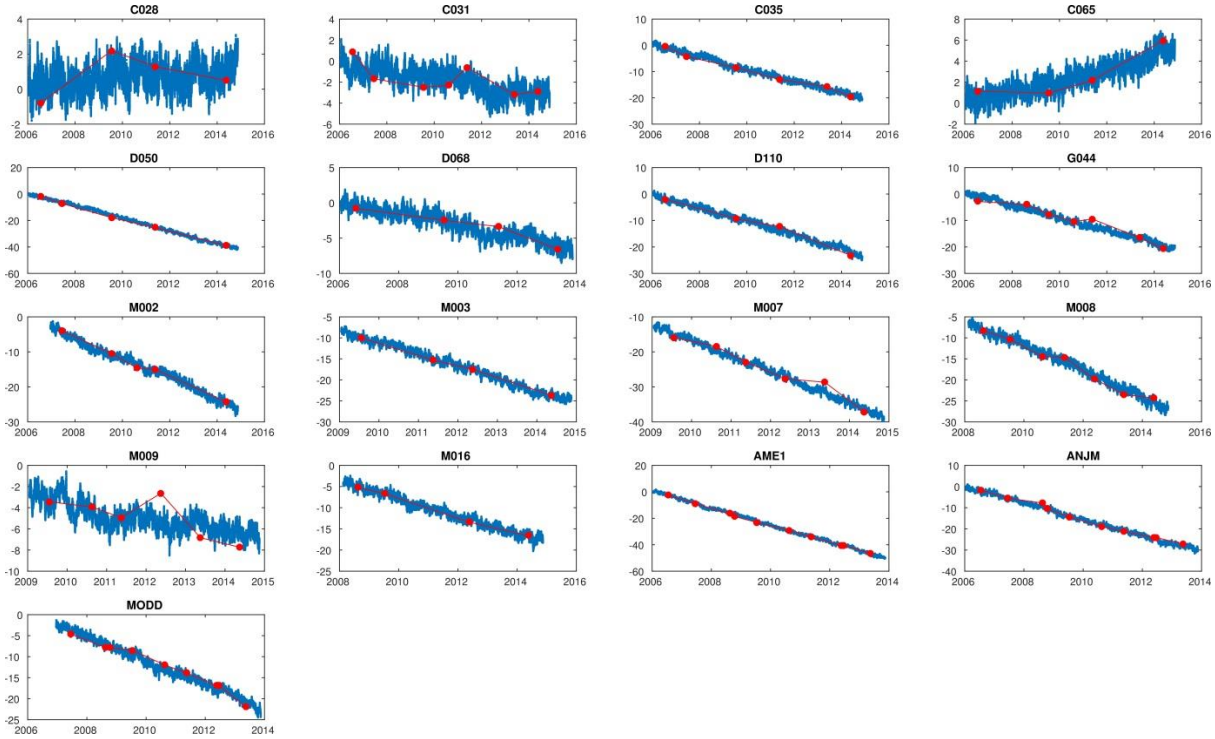

Figure 14. Height time series for the campaign (plus AME1, ANJM and MODD) sites that have four or more measurements. Red circles are the campaign measurements. Blue dots are synthetic continuous time series derived from the modified 06-GPS/NAM model to highlight the additional "set up" noise the campaign sites suffer from.

The agreement between the standard deviations from the simulated data and the residuals indicates that the "set up" error can be considered to be quite low (< 1 mm) presumably due to the use of grouped benchmarks and optical levelling before and after the survey. Looking at the variations between time series from the clustered benchmarks we get a standard deviation of 1.5 mm. This may indicate movement of the benchmarks in the mudflats and as such this would be an additional temporally correlated noise that we have no means yet to investigate. We should also bear in mind that simply removing and replacing the same antenna can produce offsets on the order of 1 mm. Therefore to err on the side of cautious we should assign a "set up" error of at least 1 mm and note that the errors may still be over optimistic because we cannot yet account the temporal effects of benchmark movement (which has, from limited calculations a standard deviation of 1.5 mm).

The trends for the sites plotted in Figure 14 are also shown in Table 9 below. The trend in the first column is calculated just using the covariance derived from model #6 of the continuous height time

series whereas the second column includes the 1 mm white noise set up error. The 1 mm setup error adds about 25% to the uncertainty (which will decrease with time). Note that no attempt has been made to scale up the uncertainties based on the residual fit.

Table 9. Trends and uncertainties for the campaign sites with 4 or more measurements. Also included are the "campaign" results for the three continuous sites AME1, ANJM, and MODD. First column is the uncertainties based on model 6 of the vertical continuous time series. Second column includes a set up noise equivalent to 1 mm of white noise.

Site	Trend (mm/yr)	Trend (mm/yr)	Site	Trend (mm/yr)	Trend (mm/yr)
C028	0.14 ± 0.23	0.14 ± 0.29	M003	-2.81 ± 0.37	-2.81 ± 0.46
C031	-0.37 ± 0.20	-0.36 ± 0.25	M007	-4.25 ± 0.34	-4.25 ± 0.42
C035	-2.29 ± 0.20	-2.28 ± 0.25	M008	-2.99 ± 0.22	-2.99 ± 0.30
C065	0.60 ± 0.23	0.61 ± 0.29	M009	-0.85 ± 0.34	-0.84 ± 0.42
D050	-4.70 ± 0.22	-4.69 ± 0.27	M016	-2.02 ± 0.24	-2.04 ± 0.32
D068	-0.80 ± 0.26	-0.80 ± 0.33	AME1	-6.36 ± 0.22	-6.36 ± 0.27
D110	-2.65 ± 0.23	-2.65 ± 0.29	ANJM	-3.80 ± 0.22	-3.81 ± 0.27
G044	-2.26 ± 0.21	-2.27 ± 0.26	MODD	-2.76 ± 0.27	-2.75 ± 0.32
M002	-2.91 ± 0.26	-2.91 ± 0.32			

Periodic Signals in Campaign Data

In the continuous data any periodic signals can be accounted for in the least squares so long as the length of the time series is sufficiently long, and the sampling period sufficiently small, compared to the period of the signal [*Blewitt and Lavallee*, 2002]. However for campaign data, particularly campaigns that are annual in nature, the periodic signals cannot be estimated and will propagate directly into an error in the trend. Therefore instead of estimating the periodic signal we have to account for it in the error budget. Additionally the campaign data presented here are an average taken over several days (typically 3 – 5 days) so any residual tidal signals may have an impact on the average. We will examine these two issues in this section

Aliasing of tidal signatures

We can see from figures 3, 4 and 7 that there is significant power at tidal frequencies particularly at K1, K2 and their harmonics. [*Penna and Stewart*, 2003; *Penna et al.*, 2007] have shown that tidal signals can alias into long period signals but that was mainly for continuous daily data. We took the vertical component from AME1, ANJM and MODD and estimated the amplitude and phase for the dominant tidal frequencies (plus extra harmonics of K1). Although they are obviously significant in the power spectrum the maximum signal is 0.05 mm for K1 in ANJM. Overall, the 99th to 1st percentile range for the predicted sub-daily tidal signal is 0.12 – 0.15 mm for the three sites. If we take the predicted tidal signal from the least squares we can use this to estimate the effect those signals have on the 3-day or 5-day mean. We find that averaging over three days can bias the result by less than 0.001 mm and less than 0.0006 mm for a 5-day average. So we can safely ignore the aliasing of sub-daily tidal signals on the campaign averages.

Aliasing of long period signals on the trend

The Wadden Sea campaigns are generally performed once per year starting at approximately the same time each year. Not every benchmark is included in every survey campaign, but surveyed at least once

every three years. Also due to logistical restrictions of measuring in the sea only 1 – 3 antennas can be mounted or un-mounted every day leading to a rolling, partly overlapping, occupation of the benchmarks. If we have purely sinusoidal signal and surveys performed at exactly the same time each year then the signal would have no effect on the trend estimate. If they are not surveyed at exactly the same time (or the signal is not a pure sinusoid) then this will propagate into the trend. An example is shown in Figure 15 below.

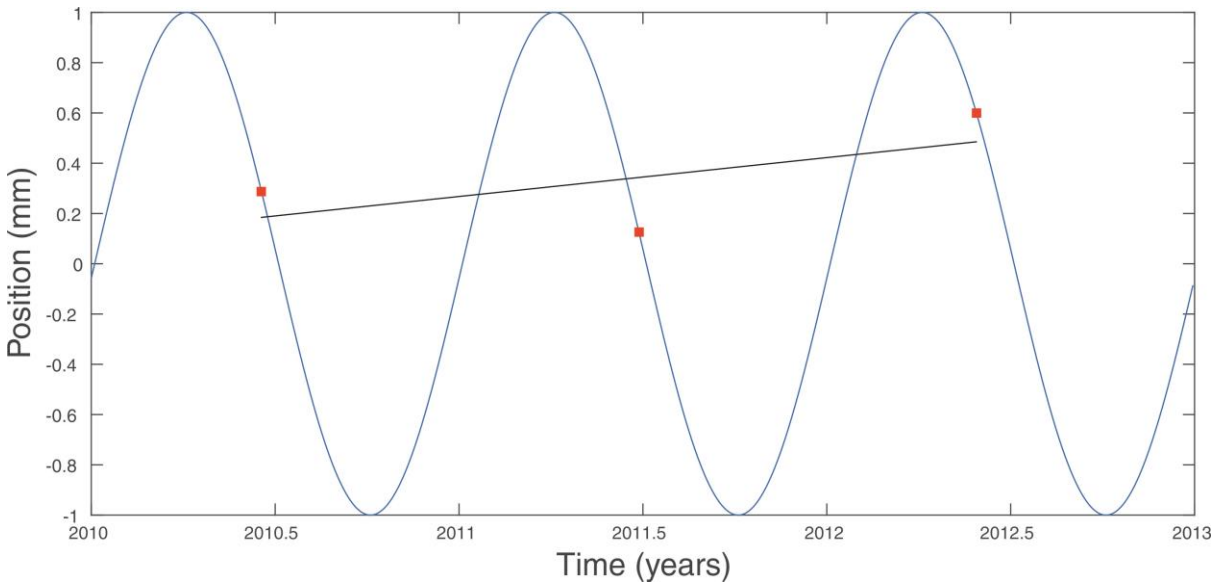

Figure 15. Effect of sampling a periodic signal at uneven times of the year. The blue line is the actual periodic signal and the red line is three years of measurements at day of year 170, 180 and 150. The black line is the least squares fit to the three points showing a non-zero trend of 0.15 mm/yr.

To examine the effect this has on the campaign sites we run Monte Carlo simulations (10000) per site using the measurement dates given for each site. For each simulation we kept the amplitude of the annual signal at 1mm and varied the phase of the signal. We then estimated an intercept and trend for each simulation and took the standard deviation of all the trends. The results are plotted as red squares in Figure 16 below. The blue line in Figure 16 is the estimated uncertainty from Monte Carlo simulation from a series with the given time span for just two measurements. We see that the dominant effect is the length of the time series, with second order effects being the individual positions and number of campaigns per site. From the least squares fit to the vertical time series of AME1, ANJM and MODD we get a very small annual signal of 0.35 mm, 0.19 mm and 0.15 mm respectively. For the worst case in Figure 16, site H044 with a time span of 2 years and 277 days, the uncertainty due to an annual signal of 0.35 mm is 0.12 mm/yr. It turns out that we can form the equation for the uncertainty as

$$\sigma_r = \frac{\sqrt{2}a}{T}|\sin \pi f T| \tag{11}$$

where a is the amplitude of the periodic signal, T is the length of the measurements (in years) and f is the frequency of the periodic signal (in yrs^{-1}).

Finally there is one other effect to be wary of particularly for the annual signal. If the annual signal is common across the whole area and because the campaigns are measured at approximately the same time each year then the bias may be correlated at all sites i.e. the trends may all report a trend too high or a trend too low. However, looking at the phase of the annual signal in AME1, ANJM, and MODD

there is no reason to believe that the signal is common – as we would suspect from the processing methodology where any common mode is supressed by the fixing of the reference sites.

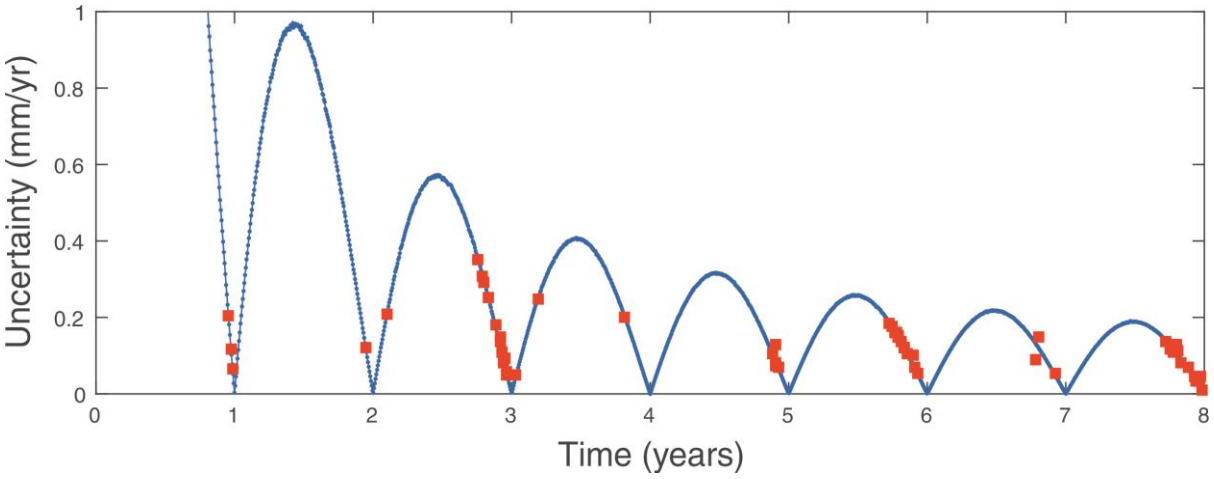

Figure 16: Uncertainty in the trend as a function of the time span of campaign data due to an annual signal of amplitude 1 mm. Blue line is the Monte Carlo derived estimate based on an annual signal with random phase for a line with two measurements. Red squares are Monte Carlo simulations with spacing of measurements equivalent to the campaign dataset.

Recommendations on Calculating GPS Uncertainties

The work in this paper has thoroughly examined the scientific literature on uncertainties in GPS coordinate time series from the start of GPS measurements through to our most recent understanding. We find that daily GPS coordinate time series are found to be, in general, a combination of temporally coloured noise (typically close to flicker noise) and white noise. The scale of the noise in the vertical is larger than the horizontal although the magnitude has steadily decreased with time due to improved models, processing, satellites and ground stations. The magnitude of the noise is also dependent on the size of the network (global, unfiltered through regional, filtered to short baseline studies) and the processing methods employed.

The GPS solution provided by 06-GPS are hourly coordinate time series and have been analysed stochastically to produce a stochastic model to be used to calculate uncertainties in parameters derived from the GPS solutions, for example trends. They results have also be compared to alternative reference time series in the region including the results from the Leica CrossCheck service. Given the analysis of the data we recommend the following

1. For the continuous data, unless the data is longer than 2½ years, do not estimate an annual and semi-annual signal in the least squares [*Blewitt and Lavallee*, 2002].
2. For the vertical data we recommend using model #6 as the default model for the data. This model combines the general model (#1) for the data based on the three longest time series and adds a secondary component that forces the stochastic model to mimic a regional filtered network at long periods.
3. For the horizontal data we recommend model #3 which is equivalent to model #6 for the vertical data.

4. To account for spatial correlations in the continuous data, first estimate the trend uncertainties using the models above. Then use equation (10) to create a correlation matrix for the spatial correlations based on the distance between the sites and the decay parameter, ρ. The covariance matrix for the trends is then calculated using the following:

$$C_{i,j} = corr_{i,j}\,\sigma_r(i)\sigma_r(j) \tag{12}$$

   where $C_{i,j}$ is the covariance between site *i* and *j*, $corr_{i,j}$ is the correlation from eq. 10 and σ_r are the trend uncertainties from sites *i* and j.

5. For the campaign data, the models for the continuous data should also be used but propagated to produce the covariance between the individual surveys. Each individual survey is an average of the hourly values from the survey period – nominally 5 days. An additional set-up noise of 1 mm (white noise) can be added to account for errors in the re-establishment of the benchmark. Spatial correlations are added in as above.
6. Errors in the average coordinate per survey are unlikely to be affected by residual tidal signals and so can be ignored.
7. Periodic signals such as the annual and semi-annual will affect the trend estimate and the size of the uncertainty is primarily a function of the length of the time series and amplitude of the signal. Uncertainties estimated using equation (11) can be added in quadrature to the calculated trend uncertainties calculated from point 5.

Recommendations on the Current Processing Approach

The literature review conducted above, together with the analysis of the 06-GPS time series, the Leica CrossCheck data and supplementary data from GNSS analysis centres in the scientific community highlight a large discrepancy between the processing approaches employed. 06-GPS use the Geo++ GNNET (GNSMART) software which uses a set of fixed reference stations surrounding the network and then estimates the coordinates of the network via a Kalman filter. Whilst, at first glance, the 06-GPS results would appear to be more precise than the equivalent scientific results it is hard to reconcile this with the literature. The nature of the processing and the size of the network would imply that the results would be equivalent to a small, filtered network. However the derived stochastic parameters would suggest the noise level is around or below that found for (< 1km) short baseline studies which are not easy to explain considering the size of the network. This, and the spectral shape at high frequencies, would suggest the Kalman filter is potentially constraining the coordinates too tightly. How this tight constraint affects any long wavelength deformation (spatially and temporally) is unknown.

The offset seen in the horizontal coordinates in May 2009 related to a change in the coordinates of several of the fixed reference stations at that time suggest a major drawback in the processing methodology with those changes in coordinates propagating into unwanted changes in the monitoring sites. Indeed for ANJM and MODD in the north component the preferred linear model was one where the trends themselves changed at this time. The offset in Feb 2014 appears to be related to the addition

of other sites in the network. This sort of effect has been seen in processing in the past as the baselines that are processed change with the addition of new sites for example. It is however something to investigate as small offsets can bias estimated trends [*Gazeaux et al.*, 2013; *S. D. P. Williams*, 2003]

[*Geng et al.*, 2012; *S. D. P. Williams and Penna*, 2011] showed that known loading due to the atmosphere and ocean is detectable in GPS coordinate time series. That they are not visible (despite being on the order of 20-30 mm during severe storm surges which last from hours to a few days: the December 5/6 2013 storm surge for instance predicts a loading signal of 30 mm at AME1) in the 06-GPS time series suggests that the coordinates cannot be considered to be absolute but are instead relative (or pseudo-baseline). Even so, the relative deformation at AME1 (relative to a common mode signal from the reference sites) is estimated to be 6.6 mm and is not visible in the time series (See Figure 17 below). One could conclude that the deformation at these periods is perhaps biased by the tight constraint, the fixed reference sites or both.

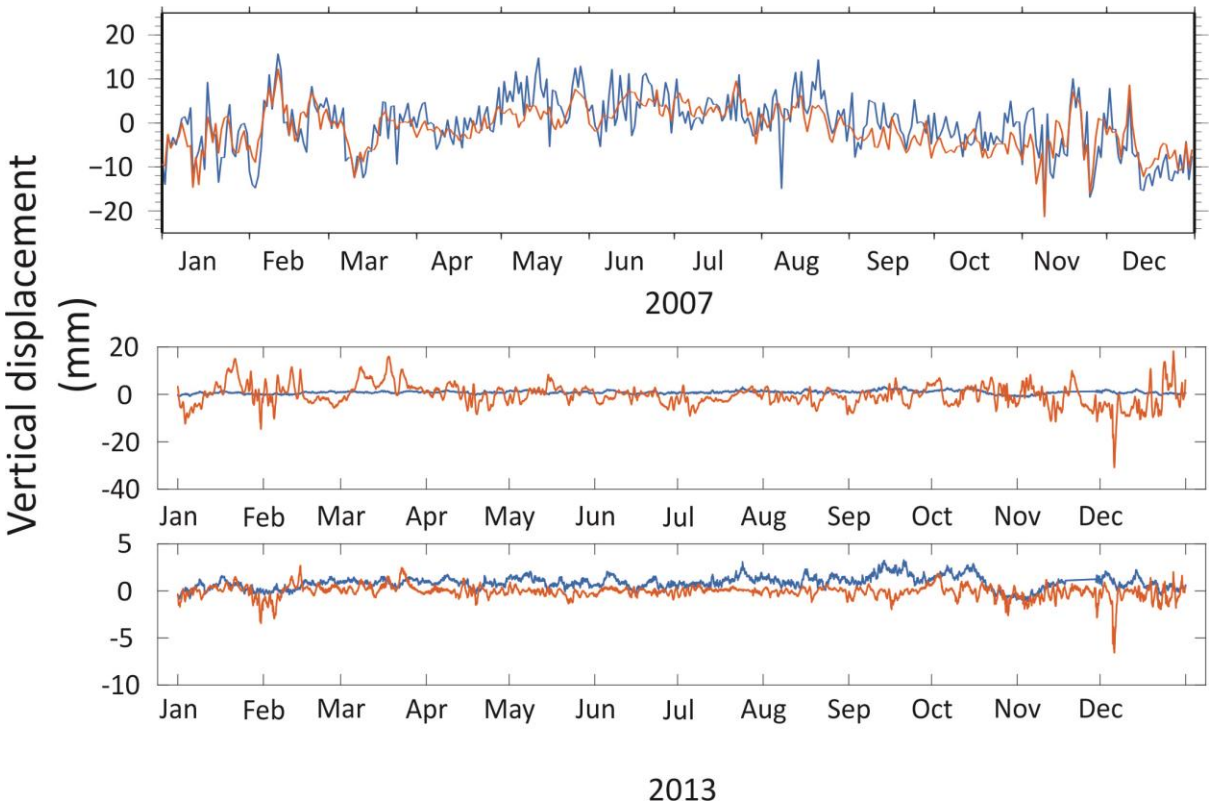

Figure 17. Vertical deformation due to atmospheric and non-tidal ocean loading. Top. Blue line is the observed deformation at TERS in 2007 from a Gipsy PPP solution. Orange line is the predicted loading deformation. Middle. Blue line is the vertical deformation for AME1 from the 06-GPS solution in 2013. Orange line is the predicted loading deformation. Note the large negative peak in December 2013. Bottom. Blue line is the vertical deformation for AME1 from the 06-GPS solution in2013. Orange line is the predicted residual loading deformation after a common mode due to the loading is removed. The peak is reduced but still large in December 2013.

Finally the break in slope of the power spectrum has to be explained. It is not seen in regular scientific processing time series but you could argue that this is because the noise in those series is higher at those frequencies. However other researchers have found flicker noise down to 1Hz [*Bock et al.*, 2000]. A break in the power-law with the high frequency spectral index close to -2 is symptomatic of some form of filtering.

The following are some recommendations on the current processing approach

1. Investigate the constraints applied to the coordinates of the continuous monitoring stations.
2. Examine the methods applied to the fixed reference sites. Absolute fixing of the site coordinates with occasional corrections to the coordinates after a separate analysis is not the optimal way to capture any differential motion at those reference sites. One should adopt a methodology similar to the IGS in its definition of the International Terrestrial Reference Frame (ITRF) whereby the reference sites are given a position and a velocity (based on a separate processing of the whole dataset of the fixed sites with respect to ITRF or EUREF).
3. If there is no real requirement for hourly solutions then we suggest moving to daily. Currently, any subdaily variations are likely effected by the kalman filter. The remaining tidal signatures seen in the subdaily may come from a variety of sources and are not indicative of the ability of the software to capture subdaily motion.
4. Consider performing a test at a site considered to be sufficiently far away from any subsidence where you can move the antenna in a known and easily measured (not via GPS) manner continuously over a period of time sufficiently long enough to be lower than the cross over frequency seen in the data (and not related to any known tidal period). We would suggest something on the order of 100 days and resembling a sawtooth function so that it is easily verifiable.
5. Switch to or use in parallel the Leica CrossCheck service. The results from this service have shown to be in line with the results from the scientific community and therefore have an established track record. One obvious drawback to this is that the service is a black box system and therefore potential problems with the data will be harder to track down than specialised processing of the data

The views expressed in this paper are those of the author and do not necessarily reflect the policies of the National Oceanography Centre.

References

Agnew, D. C. (1992), The Time-Domain Behavior of Power-Law Noises, *Geophys Res Lett*, *19*(4), 333-336.

Allan, D. W. (1966), Statistics of atomic frequency standards, *Proc. IEEE*, *54*, 221-230.

Amiri-Simkooei, A. (2009), Noise in multivariate GPS position time-series, *J Geod*, *83*(2), 175-187.

Amiri-Simkooei, A. R., C. C. J. M. Tiberius, and P. J. G. Teunissen (2007), Assessment of noise in GPS coordinate time series: Methodology and results, *Journal of Geophysical Research -Solid Earth*, *112*(B07413).

Beavan, J. (2005), Noise properties of continuous GPS data from concrete pillar geodetic monuments in New Zealand and comparison with data from U.S. deep drilled braced monuments, *J. Geophys. Res.-Solid Earth*, *110*(B8).

Beran, J. (1994), *Statistics for Long-Memory Processes*, Taylor & Francis.

Blewitt, G., and D. Lavallee (2002), Effect of annual signals on geodetic velocity, *J. Geophys. Res.-Solid Earth*, *107*(B7), art. no.-2145.

Bock, Y., R. M. Nikolaidis, P. J. de Jonge, and M. Bevis (2000), Instantaneous geodetic positioning at medium distances with the Global Positioning System, *J. Geophys. Res.-Solid Earth*, *105*(B12), 28223-28253.
Bos, M., R. Fernandes, S. Williams, and L. Bastos (2008), Fast error analysis of continuous GPS observations, *Journal of Geodesy*, *82*(3), 157-166.
Bos, M. S., L. Bastos, and R. M. S. Fernandes (2010), The influence of seasonal signals on the estimation of the tectonic motion in short continuous GPS time-series, *Journal of Geodynamics*, *49*(3-4), 205-209.
Bos, M. S., R. M. S. Fernandes, S. D. P. Williams, and L. Bastos (2013), Fast error analysis of continuous GNSS observations with missing data, *J Geod*, 1-10.
Bos, M. S., S. D. P. Williams, I. B. Araújo, and L. Bastos (2014), The effect of temporal correlated noise on the sea level rate and acceleration uncertainty, *Geophysical Journal International*, *196*(3), 1423-1430.
Bottiglieri, M., M. Falanga, U. Tammaro, P. De Martino, F. Obrizzo, C. Godano, and F. Pingue (2010), Characterization of GPS time series at the Neapolitan volcanic area by statistical analysis, *J. Geophys. Res.-Solid Earth*, *115*.
Calais, E. (1999), Continuous GPS measurements across the Western Alps, 1996-1998, *Geophysical Journal International*, *138*(1), 221-230.
Calais, E., J. Y. Han, C. DeMets, and J. M. Nocquet (2006), Deformation of the North American plate interior from a decade of continuous GPS measurements, *J. Geophys. Res.-Solid Earth*, *111*(B6), 23.
Caporali, A. (2003), Average strain rate in the Italian crust inferred from a permanent GPS network - I. Statistical analysis of the time-series of permanent GPS stations, *Geophysical Journal International*, *155*, 241-253.
Davis, J. L., B. P. Wernicke, and M. E. Tamisiea (2012), On seasonal signals in geodetic time series, *J. Geophys. Res.*, *117*(B1), B01403.
Davis, J. L., W. H. Prescott, J. L. Svarc, and K. J. Wendt (1989), Assessment of Global Positioning System Measurements for Studies of Crustal Deformation, *J Geophys Res*, *94*(B10), 13635-13650.
Dmitrieva, K., P. Segall, and C. Demets (2015), Network-based estimation of time-dependent noise in GPS position time series, *J Geod*.
Dong, D., P. Fang, Y. Bock, M. K. Cheng, and S. Miyazaki (2002), Anatomy of apparent seasonal variations from GPS-derived site position time series, *J. Geophys. Res.-Solid Earth*, *107*(B4), art. no.-2075.
Gardner, M. (1978), Mathematical Games : White and brown music, fractal curves and one-over-f fluctuations, *Scientific American*, *238*(4), 16-32.
Gazeaux, J., et al. (2013), Detecting offsets in GPS time series: First results from the detection of offsets in GPS experiment, *Journal of Geophysical Research: Solid Earth*, n/a-n/a.
Geng, J., S. D. P. Williams, F. N. Teferle, and A. H. Dodson (2012), Detecting storm surge loading deformations around the southern North Sea using subdaily GPS, *Geophysical Journal International*.
Hackl, M., R. Malservisi, U. Hugentobler, and R. Wonnacott (2011), Estimation of velocity uncertainties from GPS time series: Examples from the analysis of the South African TrigNet network, *J. Geophys. Res.-Solid Earth*, *116*.
Hill, E. M., J. L. Davis, P. Elósegui, B. P. Wernicke, E. Malikowski, and N. A. Niemi (2009), Characterization of site-specific GPS errors using a short-baseline network of braced monuments at Yucca Mountain, southern Nevada, *Journal of Geophysical Research: Solid Earth*, *114*(B11), B11402.
Hosking, J. R. M. (1981), Fractional differencing, *Biometrika*, *68*(1), 165-176.

Hurst, K. J., M. B. Heflin, D. Jefferson, and F. Webb (2000), The use of a regional reference frame in realizing the inherent precision of regional GPS, *Eos Trans. AGU*, *81*(48), Fall Meet. Suppl., Abstract G12A-01.
Johnson, H. O., and F. Wyatt (1994), Geodetic network design for fault-mechanics studies, *manuscripta geodaetica*, *19*, 309-323.
Johnson, H. O., and D. C. Agnew (1995), Monument Motion and Measurements of Crustal Velocities, *Geophys Res Lett*, *22*(21), 2905-2908.
Johnson, H. O., and D. Agnew (2000), Correlated Noise in Geodetic Time Series*Rep. 1434-HQ-97-GR-03155*, USGS, San Diego.
Khan, S. A., L. Liu, J. Wahr, I. Howat, I. Joughin, T. van Dam, and K. Fleming (2010), GPS measurements of crustal uplift near Jakobshavn Isbrae due to glacial ice mass loss, *J. Geophys. Res.-Solid Earth*, *115*.
King, M., et al. (2010), Improved Constraints on Models of Glacial Isostatic Adjustment: A Review of the Contribution of Ground-Based Geodetic Observations, *Surveys in Geophysics*, *31*(5), 465-507.
King, M. A., and S. D. P. Williams (2009), Apparent stability of GPS monumentation from short-baseline time series, *J. Geophys. Res.*, *114*.
King, N. E., J. L. Svarc, E. B. Fogleman, W. K. Gross, K. W. Clark, G. D. Hamilton, C. H. Stiffler, and J. M. Sutton (1995), Continuous GPS observations across the Hayward fault, California, 1991-1994, *J Geophys Res*, *100*(B10), 20271-20283.
Langbein, J. (2004), Noise in two-color electronic distance meter measurements revisited, *J. Geophys. Res.-Solid Earth*, *109*(B4), art. no.-B04406.
Langbein, J. (2008), Noise in GPS displacement measurements from Southern California and Southern Nevada, *J. Geophys. Res.*, *113*(B5), 1-12.
Langbein, J., and H. Johnson (1997), Correlated errors in geodetic time series: Implications for time-dependent deformation, *J. Geophys. Res.-Solid Earth*, *102*(B1), 591-603.
Langbein, J., and Y. Bock (2004), High-rate real-time GPS network at Parkfield: Utility for detecting fault slip and seismic displacements, *Geophys Res Lett*, *31*(15), art. no.-L15S20.
Langbein, J., E. Quilty, and K. Breckenridge (1993), Sensitivity of crustal deformation instruments to changes in secular rate, *Geophys Res Lett*, *20*(2), 85-88.
Larson, K. M., and D. C. Agnew (1991), Application of the Global Positioning System to Crustal Deformation Measurement 1. Precision and Accuracy, *J Geophys Res*, *96*(B10), 16547-16565.
Mandelbrot, B. B., and J. W. V. Ness (1968), Fractional Brownian Motions, Fractional Noises and Applications, *Siam Review*, *10*(4), 422-437.
Mao, A. L., C. G. A. Harrison, and T. H. Dixon (1999), Noise in GPS coordinate time series, *J. Geophys. Res.-Solid Earth*, *104*(B2), 2797-2816.
Montillet, J. P., S. McClusky, and K. G. Yu (2013), Extracting Colored Noise Statistics in Time Series via Negentropy, *IEEE Signal Processing Letters*, *20*(9), 857-860.
Niu, X. J., Q. J. Chen, Q. Zhang, H. P. Zhang, J. M. Niu, K. J. Chen, C. Shi, and J. N. Liu (2014), Using Allan variance to analyze the error characteristics of GNSS positioning, *GPS Solutions*, *18*(2), 231-242.
Olivares, G., and F. N. Teferle (2013), A Bayesian Monte Carlo Markov chain method for parameter estimation of fractional differenced Gaussian processes, *Signal Processing, IEEE Transactions on*, *61*(9), 2405-2412.
Penna, N. T., and M. P. Stewart (2003), Aliased tidal signatures in continuous GPS height time series, *Geophys Res Lett*, *30*(23), 4.
Penna, N. T., M. A. King, and M. P. Stewart (2007), GPS height time series: Short-period origins of spurious long-period signals, *J. Geophys. Res.-Solid Earth*, *112*(B2), 19.
Pesci, A., G. Teza, and G. Casula (2009), Improving strain rate estimation from velocity data of non-permanent GPS stations: the Central Apennine study case (Italy), *GPS Solutions*, *13*(4), 249-261.

Pesci, A., G. Teza, G. Casula, N. Cenni, and F. Loddo (2010), Non-permanent GPS data for regional-scale kinematics: reliable deformation rate before the 6 April, 2009, earthquake in the L'Aquila area, *Annals of Geophysics*, *53*(2), 55-68.
Ray, J., Z. Altamimi, X. Collilieux, and T. Van Dam (2008), Anomalous harmonics in the spectra of GPS position estimates, *GPS Solutions*, *12*(1), 55-64.
Santamaría-Gómez, A., M.-N. Bouin, X. Collilieux, and G. Wöppelmann (2011), Correlated errors in GPS position time series: Implications for velocity estimates, *J. Geophys. Res.*, *116*(B1), B01405.
Scargle, J. D. (1982), Studies in astronomical time series analysis. II-Statistical aspects of spectral analysis of unevenly spaced data, *The Astrophysical Journal*, *263*, 835-853.
Serpelloni, E., C. Faccenna, G. Spada, D. Dong, and S. D. P. Williams (2013), Vertical GPS ground motion rates in the Euro-Mediterranean region: New evidence of velocity gradients at different spatial scales along the Nubia-Eurasia plate boundary, *Journal of Geophysical Research: Solid Earth*, 2013JB010102.
Teferle, F. N., S. D. P. Williams, H. P. Kierulf, R. M. Bingley, and H.-P. Plag (2008), A continuous GPS coordinate time series analysis strategy for high-accuracy vertical land movements, *Physics and Chemistry of the Earth, Parts A/B/C*, *33*(3-4), 205-216.
Teza, G., A. Pesci, and G. Casula (2010), SURMODERR: A MATLAB toolbox for estimation of velocity uncertainties of a non-permanent GPS station, *Computers & Geosciences*, *36*(8), 1033-1041.
Van Dam, T., J. Wahr, P. C. D. Milly, A. B. Shmakin, G. Blewitt, D. Lavallee, and K. M. Larson (2001), Crustal displacements due to continental water loading, *Geophys Res Lett*, *28*(4), 651-654.
Voss, R. F., and J. Clarke (1975), 1/f Noise in Music and Speech, *Nature*, *258*(5533), 317-318.
Wdowinski, S., Y. Bock, J. Zhang, P. Fang, and J. Genrich (1997), Southern California Permanent GPS Geodetic Array: Spatial filtering of daily positions for estimating coseismic and postseismic displacements induced by the 1992 Landers earthquake, *J. Geophys. Res.-Solid Earth*, *102*(B8), 18057-18070.
Williams, S. (2008), CATS : GPS coordinate time series analysis software, *GPS Solutions*, *12*(2), 147-153.
Williams, S., and P. Willis (2006), Error Analysis of Weekly Station Coordinates in the DORIS Network, *J Geod*, 1-15.
Williams, S. D. P. (2003), Offsets in Global Positioning System time series, *J. Geophys. Res.-Solid Earth*, *108*(B6).
Williams, S. D. P. (2003), The effect of coloured noise on the uncertainties of rates estimated from geodetic time series, *J Geod*, *76*(9-10), 483-494.
Williams, S. D. P., and N. T. Penna (2011), Non-tidal ocean loading effects on geodetic GPS heights, *Geophys. Res. Lett.*, *38*(9), L09314.
Williams, S. D. P., Y. Bock, P. Fang, P. Jamason, R. M. Nikolaidis, L. Prawirodirdjo, M. Miller, and D. J. Johnson (2004), Error analysis of continuous GPS position time series, *J. Geophys. Res.-Solid Earth*, *109*(B3), art. no.-B03412.
Wyatt, F. (1982), Displacement of Surface Monuments - Horizontal Motion, *J Geophys Res*, *87*(NB2), 979-989.
Wyatt, F. K. (1989), Displacement of Surface Monuments - Vertical Motion, *Journal of Geophysical Research-Solid Earth and Planets*, *94*(B2), 1655-1664.
Wyatt, F. K., and D. C. Agnew (2005), The PIN1 and PIN2 GPS Sites at Pinon Flat Observatory*Rep.*, Scripps Institution of Oceanography, University of California, san Diego.
Zhang, J., Y. Bock, H. Johnson, P. Fang, S. Williams, J. Genrich, S. Wdowinski, and J. Behr (1997), Southern California Permanent GPS Geodetic Array: Error analysis of daily position estimates and site velocities, *J. Geophys. Res.-Solid Earth*, *102*(B8), 18035-18055.

Appendix A: A note on the reporting of amplitudes of the stochastic noise models

In several places in this document there are references to the scaling of the noise amplitudes, particularly Tables 1, 2 and 3. To help avoid confusion we will describe where this issue originates. In one of the original papers, [*Johnson and Wyatt*, 1994] describe the derivation of a covariance matrix by propagation of errors of a transformation matrix (see also [*S.D.P. Williams*, 2003] for a discussion of this) they scaled the transform by $\Delta T^{-\kappa/4}$, where ΔT is the sampling interval. This was done to ensure that the power spectra for any power-law with spectral index κ would cross at the same frequency given the same sampling interval and noise amplitude σ_κ. At the time of the [*Zhang et al.*, 1997] paper the covariance matrix for flicker noise was approximated using an algorithm described by [*Gardner*, 1978] for simulating such noise and the constants were chosen so that a flicker noise and random walk power spectrum cross at a period of one year when both have a sampling period of one day and equal amplitude. Since then the more general form for the covariance matrix for power-law noise was derived from [*Hosking*, 1981] and the $\Delta T^{-\kappa/4}$ scaling was adopted, particularly in the CATS software [*SDP Williams*, 2008]. More recently [*M Bos et al.*, 2008; *M S Bos et al.*, 2013] ignored the ΔT scaling in their work. Therefore it essential to state which scaling you are adopting.

With the addition of alternative noise models, such as AR(1) and band-pass filtered noise the idea of scaling the amplitudes by $\Delta T^{-\kappa/4}$ becomes nonsensical. Indeed for the FIGGM, which power-law index would you adopt? The more reasonable thing to do is drop the scaling parameter and report the amplitudes as the value that is multiplied by the transformation matrix. Note that for white noise, where $\kappa = 0$, the scaling parameter $\Delta T^{-\kappa/4}$ is 1 anyway and the amplitude is the same as the usual amplitude for white noise.

In the first section of this work, the literature review, the amplitudes are quoted with the $\Delta T^{-\kappa/4}$ (or CATS) convention for ease of comparison as are the results in Table 2 which deal only with a power-law plus white noise model. From Table 3 onwards the ΔT scaling has been avoided to ease comparison between different stochastic models. To convert between new and CATS scaling of the power-law noise amplitudes simply note that

$$\sigma_{new} = \Delta T^{-\kappa/4}\, \sigma_{CATS} \tag{A1}$$

[i] This section has been subsequently revised from the original document submitted. The analysis in the original document was based on a report on the campaign data that included heights that were not corrected for antenna offsets. This was uncovered from the original report where issues with benchmarks C028 and C035 were discussed including the 15 m horizontal change in C028 indicating the use of a different benchmark in the cluster. This revision has reduced the possible setup error down from around 5 mm to probably no more than 1 – 2 mm.